



**HAL**  
open science

# A review on hydrate composition and capability of thermodynamic modeling to predict hydrate pressure and composition

Saheb Maghsoodloo Babakhani, Baptiste Bouillot, Son Ho-Van, Jérôme Douzet, Jean-Michel Herri

## ► To cite this version:

Saheb Maghsoodloo Babakhani, Baptiste Bouillot, Son Ho-Van, Jérôme Douzet, Jean-Michel Herri. A review on hydrate composition and capability of thermodynamic modeling to predict hydrate pressure and composition. *Fluid Phase Equilibria*, 2018, 472, pp.22-38. 10.1016/j.fluid.2018.05.007 . hal-01807219

**HAL Id: hal-01807219**

**<https://hal.science/hal-01807219>**

Submitted on 4 Jun 2018

**HAL** is a multi-disciplinary open access archive for the deposit and dissemination of scientific research documents, whether they are published or not. The documents may come from teaching and research institutions in France or abroad, or from public or private research centers.

L'archive ouverte pluridisciplinaire **HAL**, est destinée au dépôt et à la diffusion de documents scientifiques de niveau recherche, publiés ou non, émanant des établissements d'enseignement et de recherche français ou étrangers, des laboratoires publics ou privés.

# 1 **A review on hydrate composition and capability of thermodynamic** 2 **modeling to predict hydrate pressure and composition**

3 Saheb Maghsoodloo Babakhani\*, Baptiste Bouillot, Son Ho-Van, Jérôme Douzet, Jean-Michel  
4 Herri

5 Ecole des Mines de Saint-Etienne, SPIN, CNRS 5307, LGF, F-42023 Saint-Etienne, France

6 \* Corresponding author: saheb.m@emse.fr

7 Keywords: gas hydrates, hydrate composition, thermodynamics, phase equilibria, modeling

8

## 9 **Abstract**

10 Gas hydrates are widely considered to be a crucial topic in oil and gas industries and attracting  
11 significant research due to potential applications such as gas storage, separation as well as water  
12 desalination. While the guest composition of hydrate phase is vital, due to the experimental  
13 difficulties in measuring hydrate composition, very little applicable information is available in the  
14 literature. Paradoxically, this is true, in spite of that; completing an experimental database on  
15 hydrate composition could have a significant impact on the processes design and modeling.  
16 Moreover, this should provide fundamental knowledge of kinetic effects as well as clarifying  
17 thermodynamic equilibrium. Hence, this paper was planned with the intent to fill in the gaps,  
18 classify and offer an overview of experimentally derived data on hydrate composition for  
19 literature. In addition, a thermodynamic model based on the van der Waals and Platteeuw  
20 approach and Kihara potential was utilized to simulate the hydrate composition along with  
21 equilibrium pressure.

22 Previous experimental data shows that guest distribution in hydrate phase depends noticeably on  
23 the guest composition in vapor phase. In addition, composition of larger molecules, such as  
24 propane or butane, in the hydrate phase, is notably higher than in vapor phase. Our simulation  
25 results demonstrated that the hydrate composition data from direct measurement (microscopic  
26 tools) have been well evaluated by the thermodynamic model. Nevertheless, when structural  
27 transition can occur in a system, the thermodynamic model is no longer accurate. In the case of  
28 indirect measurements, the thermodynamic model usually predicts well the hydrate composition.  
29 Nonetheless, its capability does vary with differing hydrate composition and equilibrium  
30 pressure, to the extent that in some cases, it completely fails to predict hydrate composition. This  
31 could be due to kinetic effects on the enclathration of guest molecules during the crystallization,  
32 errors in experimental techniques to measure the hydrate composition or the model parameters  
33 like Kihara potential are not properly applied. Finally, these observations show that more reliable  
34 experimental database is needed to study the evolution of guest distribution in hydrate phase and  
35 some enhancements are required for the standard thermodynamic model.

## 36 **1. Introduction**

37 One of the main concerns in flow assurance during oil and gas production is avoiding gas hydrate  
38 formation due to the presence of water and light hydrocarbons at high pressure and low  
39 temperature conditions, especially true for deep sea drilling or arctic exploration and pipelines.  
40 Therefore, the safety and economic costs of removing gas hydrates have been of great interest [1–  
41 8]. Plus, the enormous amount of natural gas in the form of oceanic and permafrost gas hydrates  
42 are a promising future energy resource [9–12]. Recently, gas hydrates have attracted widespread  
43 attention due to diverse applications such as gas separation [13–21], CO<sub>2</sub> capture [22–30], water  
44 desalination [31–38], natural gas storage and transportation [39–44] and even planetary science  
45 [45–48]. For all above mentioned applications of clathrate hydrates, it is essential to increase our  
46 knowledge of thermodynamics, kinetics and the crystallization mechanisms of clathrate hydrates.

47 Numerous studies have investigated phase equilibria of clathrate hydrates [12,33,49–54].  
48 Nonetheless, there has been little consideration for hydrate composition. Indeed, quantifying  
49 hydrate equilibrium composition presents several obstacles such as water occlusion,  
50 heterogeneous solid phase and measuring of solid phase concentration [12]. Hence, experimental  
51 data on hydrate composition has been rare. However, these publications do include some valuable  
52 information about fundamental hydrate phase composition, enclathration process as well as guest  
53 distribution in hydrate phase. Thus, we were able to collect invaluable data from the literature  
54 about the guest distribution in hydrate phase over a wide range of temperature, pressure and  
55 compositions. Furthermore, a thermodynamic model based on van der Waals and Platteeuw  
56 approach (vdWP) was used to detect divergences from this standard approach and previous  
57 experiments. Differences will be discussed, considering that experimental data may not be at  
58 thermodynamic equilibrium.

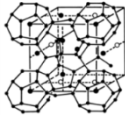
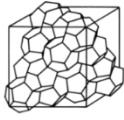
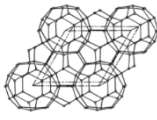
## 59 **2. Gas hydrates**

60 Water molecules in presence of gas molecules at high pressure and low temperature can form  
61 cavities and guest molecules like CO<sub>2</sub>, N<sub>2</sub>, CH<sub>4</sub>, C<sub>2</sub>H<sub>6</sub> etc. can be encased into these cavities. This  
62 ice-like structure is called gas hydrate. Based on the type of cavities and also the nature of guest  
63 molecules, there are three principal structures, sI, sII and sH. The sI usually forms in presence of  
64 small molecules (diameter between 4.2 and 6 Å) like methane and carbon dioxide. Larger  
65 molecules (diameter between 6 and 7 Å) like propane, or small molecules (diameter less than 4.2  
66 Å), such as nitrogen, form sII. sH is composed of a combination of small and large molecules  
67 (typically between 7 and 9 Å) [1,2]. Table 1 presents the differences between structures.

68

69

Table 1. The differences between three structures of gas hydrates [12]

Hydrate structures	sI		sII		sH		
Shape							
Cavity	Small	Large	Small	Large	Small	Medium	Large
Description	5 <sup>12</sup>	5 <sup>12</sup> 6 <sup>2</sup>	5 <sup>12</sup>	5 <sup>12</sup> 6 <sup>4</sup>	5 <sup>12</sup>	4 <sup>3</sup> 5 <sup>6</sup> 6 <sup>3</sup>	5 <sup>12</sup> 6 <sup>8</sup>
Number per unit cell (m <sub>i</sub> )	2	6	16	8	3	2	1
Average cavity radius (Å)	3.95	4.33	3.91	4.73	3.91	4.06	5.71
Coordination number <sup>a</sup>	20	24	20	28	20	20	36
(a) The number of oxygen atom per cavity							

71

### 72 3. Thermodynamic modeling

73 At thermodynamic equilibrium, the chemical potential of each phase must be the same. In the  
 74 case of gas hydrates, based on the classical van der Waals and Platteeuw model [55], liquid-  
 75 hydrate equilibrium is expressed by defining a metastable phase  $\beta$ , corresponding to the empty  
 76 hydrate:

$$77 \Delta\mu_W^{L-\beta} = \Delta\mu_W^{H-\beta} \quad (1)$$

78 The left hand side of equation 1 is the difference between chemical potential of water in liquid  
 79 and  $\beta$  phase and the right hand side is the difference between chemical potential of water in  
 80 hydrate and  $\beta$  phase.

#### 81 3.1. Description of $\Delta\mu_W^{L-\beta}$

82 The difference between chemical potential of water in liquid phase and  $\beta$  phase can be described  
 83 by classical thermodynamic using Gibbs-Duhem equation. It can be rewritten as follow [14]:

$$84 \Delta\mu_W^{L-\beta} =$$

$$85 T \frac{\Delta\mu_W^{L-\beta}|_{T^0 P^0}}{T^0} + \left( b_{P,W}^{L-\beta} T^0 - \Delta C_{p,w}^{L-\beta} \Big|_{P^0 T^0} \right) - T \ln \frac{T}{T^0} + \frac{1}{2} b_{P,W}^{L-\beta} T (T - T^0) + \left( \Delta h_{W,m}^{L-\beta} \Big|_{P^0 T^0} + \right.$$

$$86 T^0 \left( b_{P,W}^{L-\beta} T^0 - \Delta C_{p,w}^{L-\beta} \Big|_{P^0 T^0} \right) - \frac{1}{2} b_{P,W}^{L-\beta} T^0 \left. \right) \left( 1 - \frac{T}{T^0} \right) + \Delta v_{W,m}^{L-\beta} \Big|_{T^0} (P - P^0) - RT \ln x_W^L \quad (2)$$

87 where  $T^0=273.15\text{K}$  and  $P^0=0$  are the reference temperature and pressure, respectively.  $\Delta v_{W,m}^{L-\beta}$ ,  
 88  $\Delta C_{p,w}^{L-\beta}$  and  $b_{P,W}^{L-\beta}$  are thermodynamic properties of water in liquid phase and  $\beta$  phase and they  
 89 were calculated by Sloan and Koh [12].  $\Delta h_{W,m}^{L-\beta}$  and  $\Delta\mu_W^{L-\beta}$  are microscopic parameters of  
 90 hydrates and regrettably there are different values correspond to each author. Based on a previous  
 91 study of our team, it was concluded that the values from Handa and Tse are the best set for

92 modeling gas hydrates equilibrium [14,56]. All parameters are listed in Table 2. More details can  
 93 be found in the previous works of our group [14,47,57,58].

94 **Table 2. Thermodynamic properties of hydrates**

Parameters	Unit	Structure I	Structure II
$\Delta h_{W,m}^{L-\beta}$	J/mol	-5080	-5247
$\Delta v_{W,m}^{L-\beta}$	$10^{-6}\text{m}^3/\text{mol}$	4.5959	4.99644
$\Delta C_{p,w}^{L-\beta}$	J/mol/K	-38.12	-38.12
$b_{P,W}^{L-\beta}$	J/mol/K <sup>2</sup>	0.141	0.141
$\Delta\mu_W^{L-\beta}$	J/mol	1287	1068

95

### 96 3.2. Description of $\Delta\mu_W^{H-\beta}$

97 From van der Waals and Platteeuw approach, statistical thermodynamics is used to express

98  $\Delta\mu_W^{H-\beta}$ :

$$99 \Delta\mu_W^{H-\beta} = RT \sum_i v_i \ln(1 - \sum_j \theta_j^i) \quad (3)$$

100 where  $v_i$  is the number of cavities type  $i$  per mole of water.  $\theta_j^i$  is the occupancy factor of  
 101 molecule  $j$  in the cavity  $i$ . The occupancy factor can be described by considering the analogy  
 102 between gas adsorption in the three dimensional hydrate structures and two-dimensional  
 103 Langmuir adsorption [12,59].

$$104 \theta_j^i = \frac{C_j^i f_j(T,P)}{1 + \sum_j C_j^i f_j(T,P)} \quad (4)$$

105 where  $f_j(T, P)$  is the fugacity of guest molecule  $j$  at desire temperature and pressure. The value of  
 106 fugacity can be calculated by assuming equilibrium with a gas phase. Therefore, a standard  
 107 equation of state, such as Soave-Redlich-Kwong (SRK), can be used as fugacities are similar in  
 108 all phases, including vapor phase.  $C_j^i$  is the Langmuir constant of guest molecule  $j$  in the cavity  
 109 type  $i$ . The Langmuir constant depends on the interaction potential between the trapped guest  
 110 molecules and the surrounding water molecules cage, and for spherical guest-cages potentials can  
 111 be expressed as follows:

$$112 C_j^i = \frac{4\pi}{kT} \int_0^\infty \exp\left(-\frac{w(r)}{kT}\right) r^2 dr \quad (5)$$

113 where  $w(r)$  is the potential interaction between the guest molecule and the cavity based on the  
 114 distance between the gas and water molecule in the structure ( $r$ ). In our study, the potential  
 115 interaction was calculated based on the Kihara parameters as following:

$$116 w(r) = 2Z\epsilon \left[ \frac{\sigma^{12}}{R^{11}r} \left( \Delta^{10} + \frac{a}{R} \Delta^{11} \right) - \frac{\sigma^6}{R^5 r} \left( \Delta^4 + \frac{a}{R} \Delta^5 \right) \right] \quad (6)$$

117 and

$$118 \quad \Delta^N = \frac{1}{N} \left[ \left( 1 - \frac{r}{R} - \frac{a}{R} \right)^{-N} - \left( 1 + \frac{r}{R} - \frac{a}{R} \right)^{-N} \right] \quad (7)$$

119 Parameters  $\varepsilon$ ,  $\sigma$  and  $a$  are so-called Kihara parameters and they correspond to minimum energy,  
120 collision diameter and hard-core radius, respectively. The Kihara parameters for several gases  
121 were obtained in the previous studies by our group [47,57], and Sloan [60]. They are listed in  
122 Table 3.

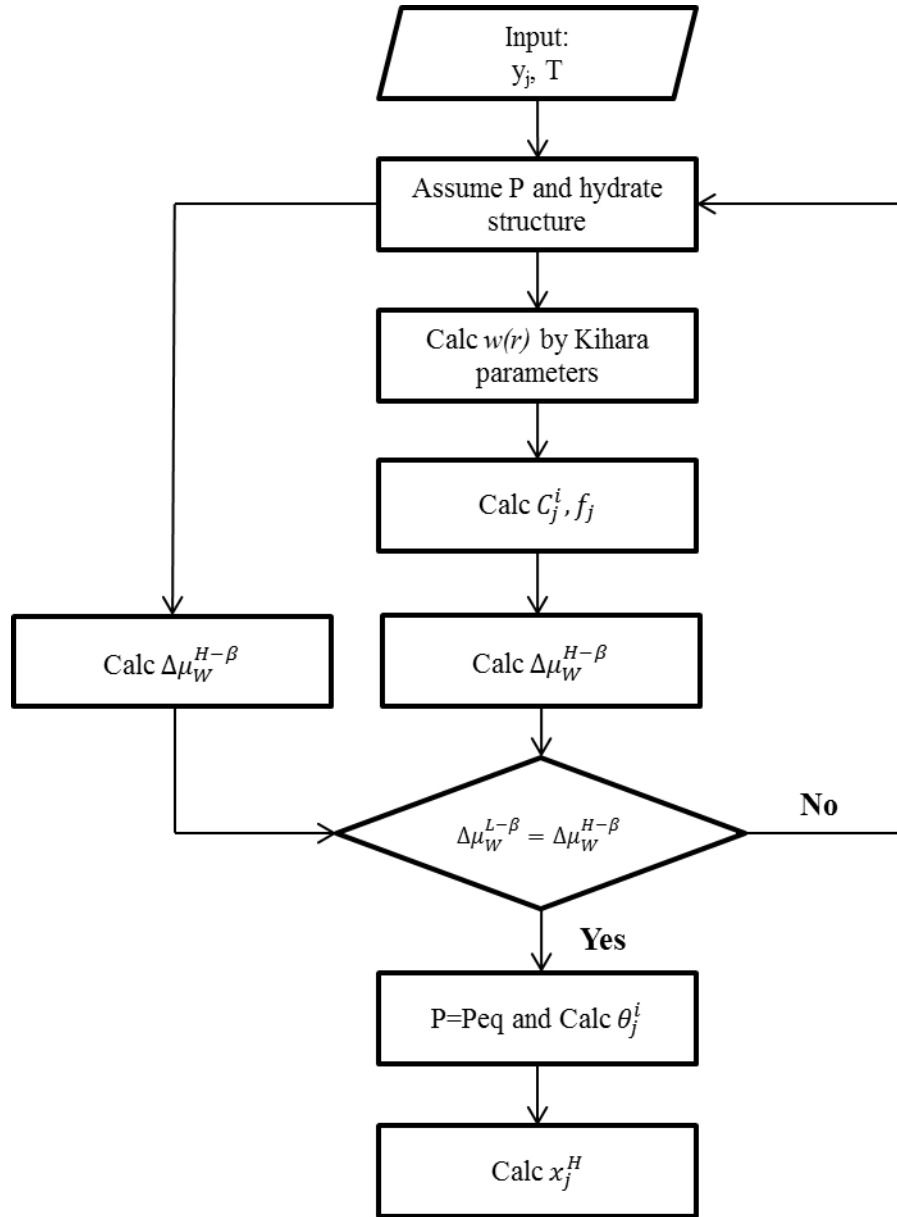
123 **Table 3. Kihara parameters for several gases.  $\varepsilon/k$ ,  $\sigma$  for  $N_2$ ,  $CO_2$ ,  $CH_4$ ,  $C_2H_6$ ,  $C_3H_8$  and  $i-C_4H_{10}$  determined**  
124 **from our earlier studies [47,57,61] and  $n-C_4H_{10}$  from Sloan [60]. Hard-core radius for all gases from Sloan**  
125 **[60]**

Gas	$\varepsilon/k$ (K)	$\sigma$ (Å)	$a$ (Å)
$N_2$	133.13	3.099	0.3526
$CO_2$	178.21	2.873	0.6805
$CH_4$	166.36	3.050	0.3834
$C_2H_6$	177.46	3.205	0.5651
$C_3H_8$	195.00	3.340	0.6502
$i-C_4H_{10}$	212.50	3.239	0.8706
$n-C_4H_{10}$	209.0	2.9125	0.9379

126  
127 First, for a gas mixture at a desired temperature, the equilibrium pressure which satisfies equation  
128 (1) is calculated. Subsequently, the occupancy factor is determined based on equation (4). Then,  
129 the hydrate composition is calculated as following:

$$130 \quad x_j^H = \frac{\sum_i v_i \theta_j^i}{\sum_i \sum_j v_i \theta_j^i} \quad (8)$$

131 The procedure for calculating hydrate equilibrium pressure and composition of mixed gas  
132 hydrates is shown in Figure 1.



133

134

**Figure 1. Procedure for calculating gas hydrate equilibrium pressure and composition**

135 The average deviations for pressure and hydrate composition have been calculated based on  
 136 equations 9 and 10, respectively.

$$137 \quad AADp\% = \frac{100}{N} \sum_i^N \left( \left| \frac{P_i^{exp} - P_i^{pre}}{P_i^{exp}} \right| \right) \quad (9)$$

$$138 \quad AADc = \frac{1}{N} \sum_i^N (|x_i^{exp} - x_i^{pre}|) \quad (10)$$

139 where  $i$  is equilibrium point,  $N$  total number of equilibrium points,  $P$  pressure,  $x$  hydrate  
 140 composition,  $exp$  experimental data and  $pre$  prediction results.  $AADp$  and  $AADc$  are average  
 141 absolute deviation for pressure and composition, respectively.

142 All the thermodynamic modelling section has been implemented in our in-house software,  
143 GasHyDyn. This software has shown a very good capability of liquid-hydrate equilibrium  
144 predictions [14,57], and will be used to discuss the experimental results for both pressure and  
145 hydrate composition. A photo from GasHyDyn environment with complementary information  
146 summarizing the procedure of submitting a calculation has been added to the Supporting  
147 Information document (Appendix A).

148 Nota Bene: the hydrate structure for modeling was chosen based on the statement of each  
149 research. Unfortunately, there were some cases that the authors did not provide the structure.  
150 Therefore, we simulated their experimental data for both structures I and II. Consequently, the  
151 structure which agreed better with the simulation results was chosen.

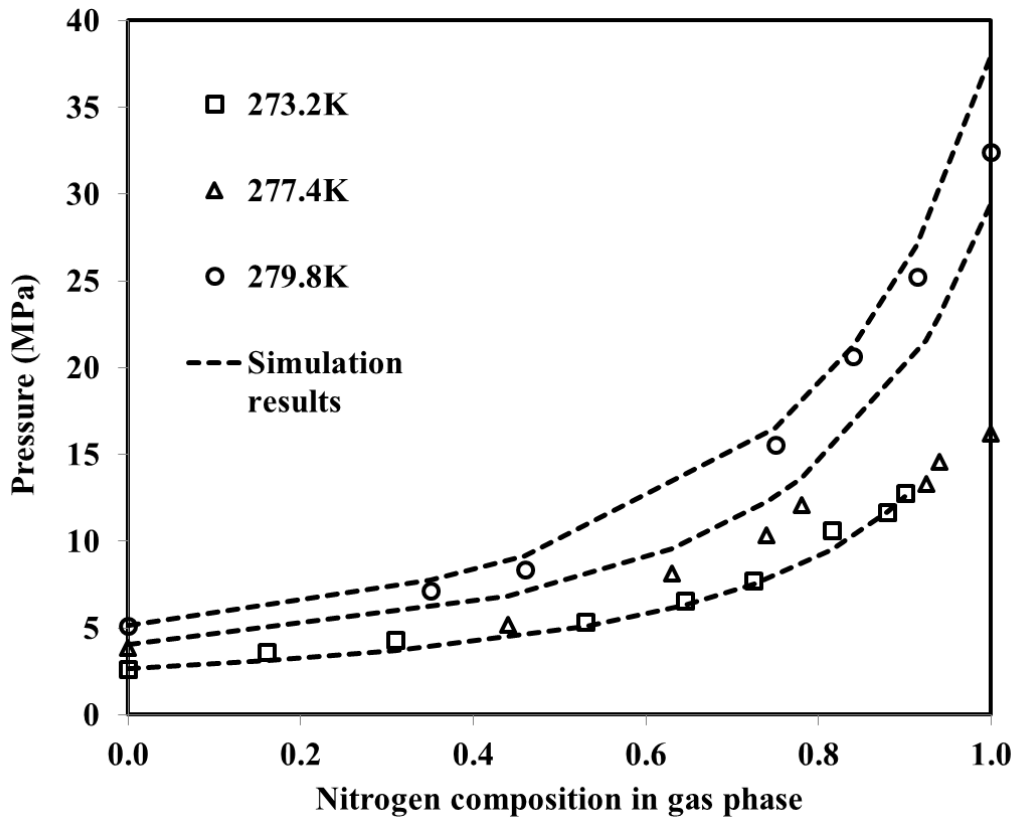
## 152 **4. Hydrate composition in literature and model comparison**

153 Despite countless works on equilibrium pressure and temperature of mixed gas hydrates, to the  
154 best of our knowledge, there are still few studies on the hydrate composition which depends on  
155 the pressure, temperature and gas phase composition. Thanks to gas chromatography, the  
156 composition of the gas phase can be easily measured, but solid phase analysis is still challenging,  
157 often leading to experimental errors. In addition, some researchers studied the hydrate  
158 composition of gas mixtures by different methods making them exceedingly difficult to compare.  
159 Hence, in the present work, studies providing hydrate composition in open literature were  
160 collected and presented. Moreover, the capability of a thermodynamic model to predict hydrate  
161 pressure and composition was evaluated. This should be noted that there were some studies on  
162 the hydrate composition of gas mixtures that do not furnish exact values of hydrate composition.  
163 Sometimes, only figures were shown and quantitative data were not available. In this section, the  
164 collected data from open literature is categorized based on their methods of hydrate composition  
165 measurements.

### 166 **4.1. Dissociation of whole hydrate phase**

167 One of the first systematic reports on the mixed hydrate composition was carried out by Jhaveri  
168 and Robinson [62]. They studied the gas hydrate equilibrium curves of methane-nitrogen mixture  
169 as well as the guest composition in gas and hydrate phases. They introduced gas mixture and  
170 water inside a batch reactor at a pressure 25% more than the equilibrium pressure at a desired  
171 temperature. After completion of hydrate formation, the gas phase was analyzed  
172 chromatographically. The gas was then removed from the reactor and the hydrate crystals  
173 dissociated. The decomposed gas was analyzed to obtain the hydrate composition. They  
174 measured hydrate composition at three temperatures 273.2, 277.4 and 279.8K for various ranges  
175 of pressure and gas compositions. Their results are illustrated in Figure 2. Clearly, at a constant  
176 temperature, by increasing the molar composition of nitrogen in the gas phase, the equilibrium  
177 pressure increased. Since the hydrate equilibrium pressure of nitrogen at a desired temperature is

178 higher than of methane. Moreover, the simulation results of equilibrium pressure were in a good  
 179 accordance with the experimental data.



180

181

Figure 2. P-x diagram of nitrogen-methane mixed hydrate (sI) [62]

182

183 **Table 4. The experimental results of Jhaveri and Robinson [62] for methane-nitrogen mixture hydrates and**  
 184 **simulation results. Uncertainties were not provided.**

Texp (K)	Pexp (MPa)	Ppre (MPa)	S	Gas composition (exp)		Hydrate composition (exp)		Hydrate composition (pre)	
				N <sub>2</sub>	CH <sub>4</sub>	N <sub>2</sub>	CH <sub>4</sub>	N <sub>2</sub>	CH <sub>4</sub>
273.2	2.640	2.660	I	0.000	1.000	0.000	1.000	0.000	1.000
273.2	3.620	3.116	I	0.160	0.840	0.065	0.935	0.034	0.966
273.2	4.310	3.708	I	0.310	0.690	0.098	0.902	0.078	0.922
273.2	5.350	5.092	I	0.530	0.470	0.200	0.800	0.176	0.824
273.2	6.550	6.301	I	0.645	0.355	0.350	0.650	0.259	0.741
273.2	7.750	7.517	I	0.725	0.275	0.425	0.575	0.339	0.661
273.2	10.640	9.525	I	0.815	0.185	0.620	0.380	0.466	0.534
273.2	11.650	11.716	I	0.880	0.120	0.710	0.290	0.597	0.403
273.2	12.770	12.577	I	0.900	0.100	0.765	0.235	0.646	0.354
277.4	3.860	4.028	I	0.000	1.000	0.000	1.000	0.000	1.000

277.4	5.200	6.839	I	0.440	0.560	0.180	0.820	0.138	0.862	
277.4	8.110	9.575	I	0.630	0.370	0.310	0.690	0.262	0.738	
277.4	10.340	12.286	I	0.740	0.260	0.470	0.530	0.378	0.622	
277.4	12.060	13.628	I	0.780	0.220	0.560	0.440	0.433	0.567	
277.4	13.320	21.582	I	0.925	0.075	0.810	0.190	0.734	0.266	
277.4	14.590	22.950	I	0.940	0.060	0.860	0.140	0.779	0.221	
277.4	16.210	29.486	I	1.000	0.000	1.000	0.000	1.000	0.000	
279.8	5.140	5.161	I	0.000	1.000	0.000	1.000	0.000	1.000	
279.8	7.140	7.751	I	0.350	0.650	0.091	0.909	0.102	0.898	
279.8	8.370	9.170	I	0.460	0.540	0.224	0.776	0.155	0.845	
279.8	15.550	16.516	I	0.750	0.250	0.550	0.450	0.404	0.596	
279.8	20.670	21.253	I	0.840	0.160	0.680	0.320	0.549	0.451	
279.8	25.230	27.054	I	0.914	0.086	0.802	0.198	0.715	0.285	
279.8	32.420	37.997	I	1.000	0.000	1.000	0.000	1.000	0.000	
AADp		16.32%	AADc					0.067		

185

186 The results of thermodynamic simulation for hydrate pressure and composition are detailed in  
187 Table 4. At 273.2 K and 279.8 K, the equilibrium pressures were successfully predicted.  
188 Nonetheless, the equilibrium pressures at 277.4 K for nitrogen compositions more than 90% mole  
189 fraction (in gas phase) were poorly simulated (sI). As nitrogen forms sII, we suspected a phase  
190 transition in this case. Hence, the experimental data were also simulated by considering sII. The  
191 results revealed that sII simulations were also unsuccessful to predict the equilibrium pressures  
192 for the 277 K isotherm at high concentrations of nitrogen in the mixture of CH<sub>4</sub>/N<sub>2</sub>. This might be  
193 due to whether the co-existence of sI and sII at this condition (which cannot be predicted by the  
194 model as it is implemented in our software) or the experimental measurement uncertainties.

195 The hydrate composition predictions were slightly different. The simulation results at low and  
196 high percentages of nitrogen in the hydrate phase agreed satisfactorily with the experimental data.  
197 But when there is no significant difference between the compositions of methane and nitrogen,  
198 the simulation results deviated from experimental. Still, the average absolute deviation of hydrate  
199 composition was less than 0.07 in mole fraction.

200 Kawasaki et al. [63] studied the guest content in hydrate phase for a gas mixture of methane,  
201 ethane, propane and iso-butane with initial molar concentrations 0.885, 0.046, 0.054 and 0.015,  
202 respectively. They used the same procedure as Jhaveri and Robinson [62] by removing the gas  
203 and dissociating the hydrate to measure the hydrate composition at two different temperatures,  
204 274.15 and 278.15 K. The experimental and simulation results are presented in Table 5.

205 **Table 5. The gas composition in different phases at 3MPa. Uncertainties were not provided.**

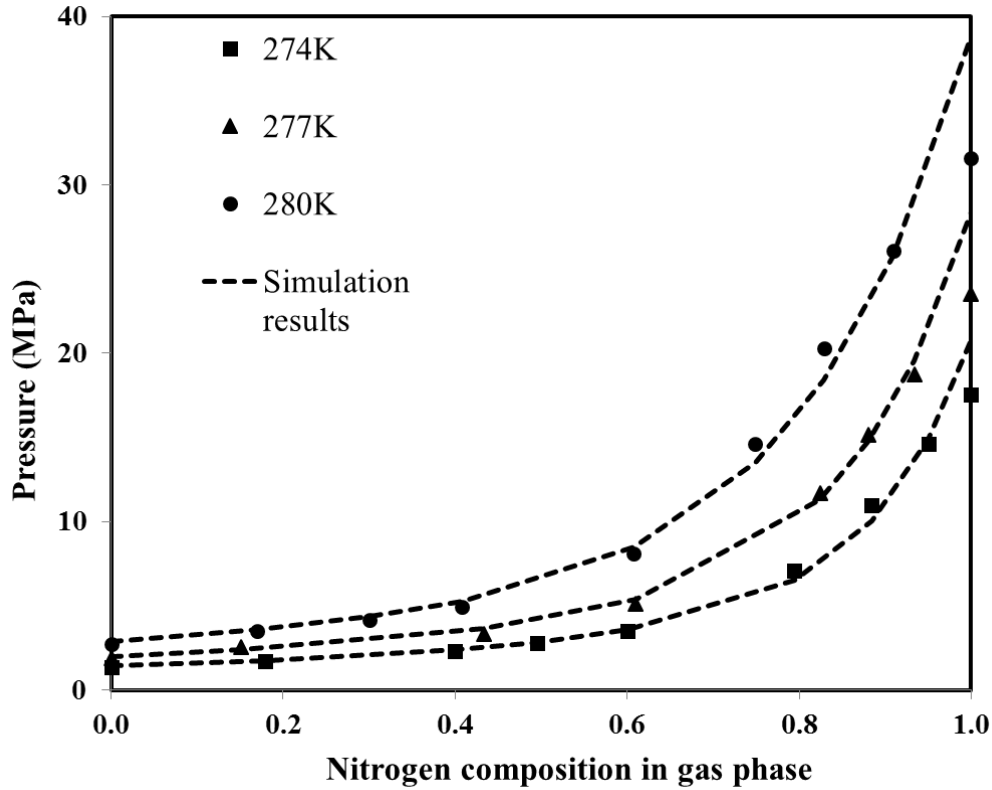
Gas	T=274.15 K		T=278.15 K	
	Gas and hydrate phase compositions		Gas and hydrate phase compositions	

	Gas (exp)	Hydrate (exp)	Hydrate (Pre)	Gas (exp)	Hydrate (exp)	Hydrate (Pre)
Methane	0.987	0.760	0.827	0.979	0.702	0.784
Ethane	0.011	0.089	0.031	0.017	0.104	0.034
Propane	0.002	0.117	0.141	0.004	0.150	0.181
iso-Butane	0.0	0.034	NA	0.0	0.044	NA

206

207 The authors remarked that all i-butane molecules concentrated in the hydrate phase, irrespective  
208 of the temperature. They also considered that the concentration of heavier hydrocarbon in hydrate  
209 phase at 278.15 K is higher at 274.15 K. Moreover, the deviation of simulation results for the  
210 hydrate composition of methane, ethane and propane were 0.074, 0.064 and 0.027, respectively.  
211 The deviations between the experimental and prediction values could be due to uncertainties in  
212 the experimental procedure. In fact, Kawasaki et al. removed the gas mixture from the reactor  
213 after hydrate formation to measure hydrate composition. Hence, the hydrate phase could be  
214 dissociated during the gas removing step due to the pressure drop, leading to the measurement  
215 uncertainties.

216 Kang et al. [64] measured the hydrate composition of CO<sub>2</sub>-N<sub>2</sub> mixture at three isotherms of  
217 vapor-hydrate equilibrium condition. After hydrate formation, they purged the gas outside the  
218 cell and dissociated the hydrate by increasing temperature. Figure 3 presents the equilibrium  
219 pressure versus nitrogen composition in the gas phase at H-V equilibrium condition for three  
220 isotherms. Our simulation results are also shown by dash lines in the figure. The simulation of  
221 hydrate composition is detailed in Table 6 as well as the experimental results.



222

223 Figure 3. Experimental H-V equilibrium data for N<sub>2</sub>/CO<sub>2</sub> mixture by Kang et al. [64] and the simulation  
224 results (sI)

225

226 Table 6. Experimental results of Kang et al. [64] and simulation. Composition uncertainties were not  
227 provided.

T <sub>exp</sub> (K) (±0.1)	P <sub>exp</sub> (MPa) (±0.01)	P <sub>pre</sub> (MPa)	S	Gas composition (exp)		Hydrate composition (exp)		Hydrate composition (pre)	
				CO <sub>2</sub>	N <sub>2</sub>	CO <sub>2</sub>	N <sub>2</sub>	CO <sub>2</sub>	N <sub>2</sub>
274.0	1.36	1.42	I	1.00	0.00	1.00	0.00	1.00	0.00
274.0	1.73	1.74	I	0.82	0.18	0.99	0.02	0.98	0.02
274.0	2.30	2.39	I	0.60	0.40	0.95	0.05	0.94	0.06
274.0	2.77	2.84	I	0.50	0.50	0.93	0.07	0.92	0.08
274.0	3.48	3.57	I	0.40	0.60	0.90	0.10	0.87	0.13
274.0	7.07	6.55	I	0.21	0.79	0.58	0.42	0.71	0.29
274.0	10.95	10.03	I	0.12	0.88	0.34	0.66	0.53	0.47
274.0	14.59	14.91	I	0.05	0.95	0.18	0.82	0.28	0.72
274.0	17.52	20.81	I	0.00	1.00	0.00	1.00	0.00	1.00
277.0	1.91	1.99	I	1.00	0.00	1.00	0.00	1.00	0.00
277.0	2.54	2.38	I	0.85	0.15	0.98	0.02	0.98	0.02
277.0	3.30	3.65	I	0.57	0.43	0.95	0.05	0.93	0.07

277.0	5.12	5.40	I	0.39	0.61	0.89	0.11	0.85	0.15	
277.0	11.71	11.30	I	0.18	0.82	0.54	0.46	0.62	0.38	
277.0	15.15	14.81	I	0.12	0.88	0.35	0.65	0.49	0.51	
277.0	18.74	19.56	I	0.07	0.93	0.19	0.81	0.31	0.69	
277.0	23.50	28.37	I	0.00	1.00	0.00	1.00	0.00	1.00	
277.0	1.91	1.99	I	1.00	0.00	1.00	0.00	1.00	0.00	
277.0	2.54	2.38	I	0.85	0.15	0.98	0.02	0.98	0.02	
280.0	2.74	2.86	I	1.00	0.00	1.00	0.00	1.00	0.00	
280.0	3.52	3.57	I	0.83	0.17	0.98	0.02	0.98	0.02	
280.0	4.14	4.35	I	0.70	0.30	0.96	0.04	0.95	0.05	
280.0	4.95	5.29	I	0.59	0.41	0.94	0.06	0.92	0.08	
280.0	8.09	8.50	I	0.39	0.61	0.86	0.14	0.83	0.17	
280.0	14.64	13.50	I	0.25	0.75	0.64	0.36	0.68	0.32	
280.0	20.29	18.39	I	0.17	0.83	0.45	0.55	0.55	0.45	
280.0	26.09	25.74	I	0.09	0.91	0.22	0.78	0.35	0.65	
280.0	31.58	38.81	I	0.00	1.00	0.00	1.00	0.00	1.00	
AADp		6.5%	AADc					0.04		

228

229 As Figure 3 and Table 6 indicate, the thermodynamic model acceptably predicted the equilibrium  
 230 pressure (average deviation 6.5%). The hydrate composition simulation could be categorized in  
 231 two parts. The first part is when carbon dioxide was dominant in the hydrate phase. In this case,  
 232 the simulation results were well predicated (average absolute deviation for 13 equilibrium points  
 233 was 0.016 mole fraction). While nitrogen was dominant in the hydrate phase, the average  
 234 absolute deviation was 0.071 in mole fraction.

#### 235 4.2. Material balance and volumetric properties evaluated from equation of state

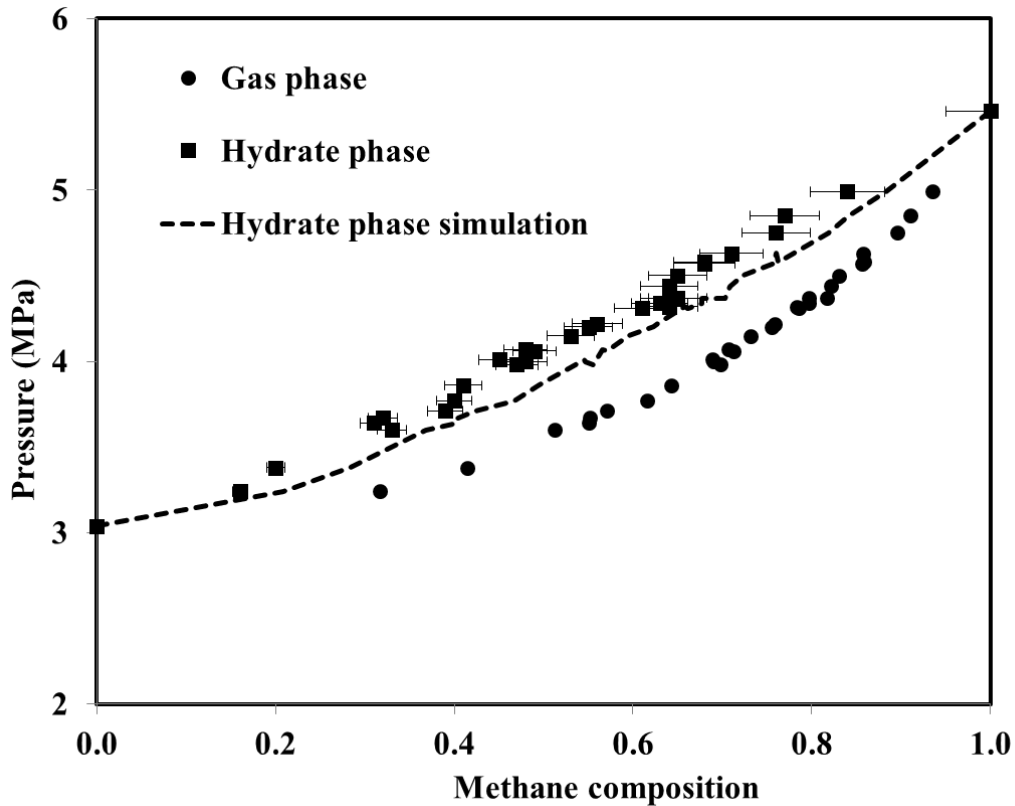
236 Ohgaki et al. investigated the phase equilibrium of carbon dioxide-methane hydrate at 280.3 K  
 237 [65]. They obtained the guest composition in gas, liquid and hydrate phases at isothermal  
 238 conditions in a batch reactor. Their experimental procedure is briefly described as follows: They  
 239 injected separately carbon dioxide and methane to the reactor. Pure water was then introduced to  
 240 the reactor. The amount of each material was weighed. Thanks to a gas chromatograph, they  
 241 determined the gas composition of carbon dioxide and methane at equilibrium temperature and  
 242 pressure. The solubility of carbon dioxide and methane in water was calculated based on Henry  
 243 constants. They assumed that the general formula for mixed carbon dioxide-methane hydrate is as  
 244 follows:

$$245 \quad zCO_2 \cdot (1 - z) \cdot qH_2O \quad (11)$$

246 where  $z$  is the mole fraction of carbon dioxide in hydrate phase and  $q$  is the hydration number at  
 247 ideal condition. They also hypothesized that the molar volume of hydrate is  $130.1 \text{ cm}^3/\text{mol}$  [65].  
 248 They calculated the volumetric properties from Soave-Redlich-Kwong equation of state or

249 IUPAC recommended equation of state for carbon dioxide and methane [60,65–67]. The hydrate  
 250 compositions were then calculated by the material balance.

251 Figure 4 shows their experimental results for hydrate phase composition and our simulation  
 252 results. Furthermore, Table 7 summarizes the experimental and modeling results by details for  
 253 carbon dioxide-methane hydrate at 280.3 K.



254

255 **Figure 4. Carbon dioxide-methane hydrates phase equilibria at 280.3 K. Experimental [65] and simulation**  
 256 **results (sI). Error bars correspond to the standard uncertainty of experimental hydrate composition.**

257 **Table 7. Experimental results of Ohgaki et al. [65] for methane-carbon dioxide mixture hydrates at 280.3 K**  
 258 **and simulation results.**

P <sub>exp</sub> (MPa) (±0.005)	P <sub>pre</sub> (MPa)	S	Gas composition (exp)		Hydrate composition (exp) (±5%)		Hydrate composition (pre)	
			CO <sub>2</sub>	CH <sub>4</sub>	CO <sub>2</sub>	CH <sub>4</sub>	CO <sub>2</sub>	CH <sub>4</sub>
3.04	2.98	I	1.00	0.00	1.00	0.00	1.00	0.00
3.24	3.46	I	0.68	0.32	0.84	0.16	0.79	0.21
3.38	3.55	I	0.59	0.42	0.80	0.20	0.72	0.28
3.60	3.85	I	0.49	0.51	0.67	0.33	0.63	0.37
3.64	3.93	I	0.45	0.55	0.69	0.31	0.60	0.40
3.67	3.93	I	0.45	0.55	0.68	0.32	0.60	0.40
3.71	3.98	I	0.43	0.57	0.61	0.39	0.58	0.42

3.77	4.09	I	0.38	0.62	0.60	0.40	0.53	0.47	
3.86	4.16	I	0.36	0.64	0.59	0.41	0.50	0.50	
4.22	4.49	I	0.24	0.76	0.44	0.56	0.37	0.63	
4.31	4.57	I	0.22	0.79	0.39	0.61	0.34	0.66	
4.32	4.57	I	0.22	0.78	0.36	0.64	0.34	0.66	
4.34	4.61	I	0.20	0.80	0.37	0.63	0.32	0.68	
4.37	4.61	I	0.20	0.80	0.35	0.65	0.32	0.68	
4.37	4.68	I	0.18	0.82	0.36	0.64	0.30	0.70	
4.44	4.70	I	0.18	0.82	0.36	0.64	0.29	0.71	
4.50	4.73	I	0.17	0.83	0.35	0.65	0.28	0.72	
4.57	4.82	I	0.14	0.86	0.32	0.68	0.24	0.76	
3.98	4.31	I	0.30	0.70	0.53	0.47	0.44	0.56	
4.00	4.29	I	0.31	0.69	0.52	0.48	0.45	0.55	
4.01	4.28	I	0.31	0.69	0.55	0.45	0.45	0.55	
4.06	4.35	I	0.29	0.71	0.51	0.49	0.43	0.57	
4.07	4.33	I	0.29	0.71	0.52	0.48	0.43	0.57	
4.15	4.41	I	0.27	0.73	0.47	0.53	0.41	0.59	
4.20	4.48	I	0.25	0.76	0.45	0.55	0.38	0.62	
4.58	4.83	I	0.14	0.86	0.32	0.68	0.24	0.76	
4.63	4.83	I	0.14	0.86	0.29	0.71	0.24	0.76	
4.75	4.96	I	0.10	0.90	0.24	0.76	0.18	0.82	
4.85	5.03	I	0.09	0.91	0.23	0.77	0.16	0.84	
4.99	5.14	I	0.07	0.94	0.16	0.84	0.12	0.88	
5.46	5.44	I	0.00	1.00	0.00	1.00	0.00	1.00	
AADp	5.8%	AADc					0.06		

259

260 They observed that at each equilibrium condition, the mole fraction of carbon dioxide in hydrate  
261 phase is significantly larger than in gas phase. Hence, based on the idea of methane exploration  
262 by carbon dioxide injection and by defining the average distribution coefficient of methane, they  
263 concluded that methane in hydrate phase can be replaced by carbon dioxide; as a result, methane  
264 concentration in the gas phase will be increased.

265 The simulation results agreed well with the experimental data for hydrate equilibrium pressure  
266 (AADp 5.8%). Additionally, the mole fraction deviation of hydrate composition calculations was  
267 about 0.06.

268 Belandria et al. investigated the compositional analysis of carbon dioxide-methane hydrate by the  
269 same method as Ohgaki et al. [65,68]. Our simulation results based on the experimental data of  
270 Belandria et al. are presented in Table 8 and Figure 5. As it is clear on the table, the  
271 thermodynamic model predicted hydrate equilibrium pressure with an acceptable error (7.8%).  
272 Although the hydrate composition simulation had mostly an adequate agreement with the data

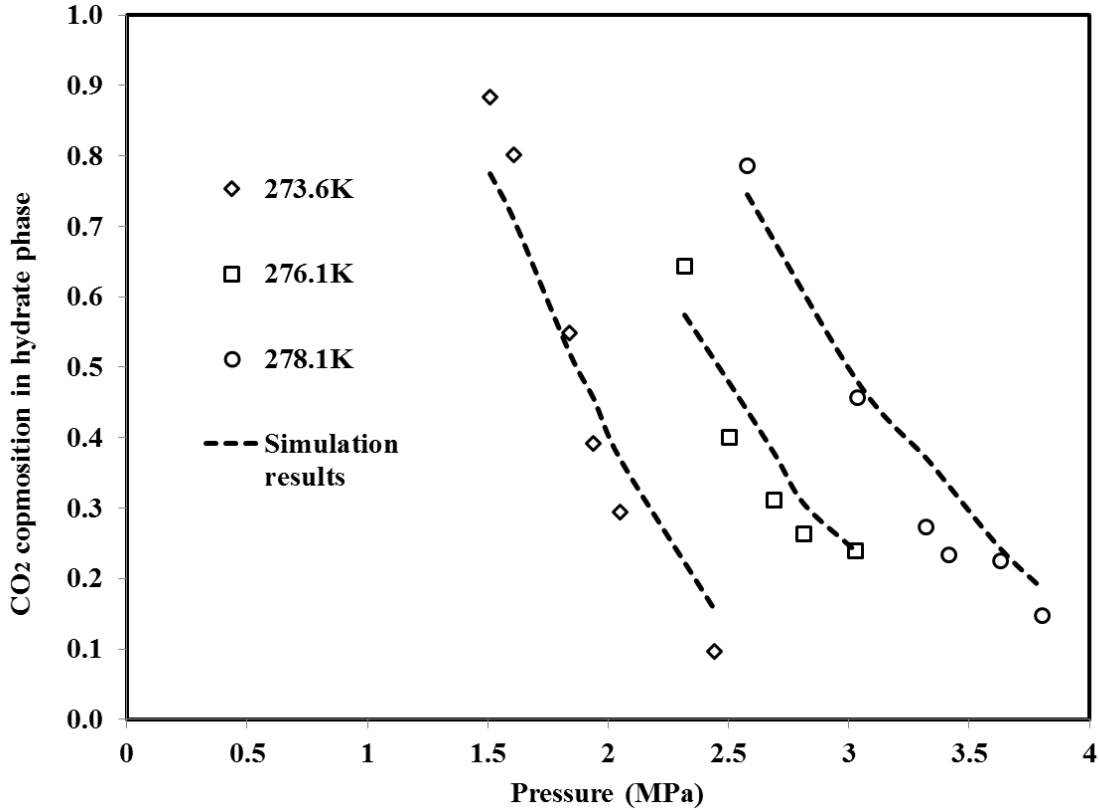
273 obtained, several experimental equilibrium points were poorly simulated (for instance 280 K and  
 274 3.54MPa). Additionally, they reported that CSMGem model was not capable to converge three  
 275 phase flash calculations in some cases, in comparison, the thermodynamic model had no problem  
 276 with three phase flash calculations [68].

277 **Table 8. Experimental results of Belandria et al. [68] for methane-carbon dioxide hydrates and simulation**  
 278 **results.**

T (K) (±0.02)	P <sub>exp</sub> (MPa) (±0.002)	P <sub>pre</sub> (MPa)	S	Gas composition (exp)		Hydrate composition (exp) (±1%)		Hydrate composition (pre)	
				CO <sub>2</sub>	CH <sub>4</sub>	CO <sub>2</sub>	CH <sub>4</sub>	CO <sub>2</sub>	CH <sub>4</sub>
273.6	2.44	2.55	I	0.08	0.92	0.10	0.90	0.16	0.84
273.6	1.84	2.03	I	0.35	0.66	0.55	0.45	0.52	0.48
273.6	1.94	2.12	I	0.29	0.71	0.39	0.61	0.46	0.54
273.6	2.05	2.24	I	0.22	0.78	0.29	0.71	0.37	0.63
273.6	1.51	1.67	I	0.63	0.37	0.88	0.12	0.77	0.23
273.6	1.61	1.77	I	0.55	0.46	0.80	0.20	0.71	0.29
275.2	2.58	2.77	I	0.17	0.83	0.34	0.66	0.29	0.71
275.2	2.77	2.98	I	0.09	0.91	0.18	0.82	0.16	0.84
275.2	2.12	2.33	I	0.38	0.62	0.65	0.35	0.56	0.44
275.2	2.22	2.48	I	0.30	0.70	0.59	0.41	0.47	0.53
275.2	2.40	2.63	I	0.23	0.77	0.37	0.63	0.38	0.62
275.2	1.79	1.96	I	0.66	0.34	0.83	0.17	0.79	0.21
275.2	1.87	2.07	I	0.57	0.44	0.75	0.25	0.72	0.28
276.1	2.81	3.00	I	0.18	0.82	0.26	0.74	0.31	0.69
276.1	3.03	3.12	I	0.13	0.87	0.24	0.76	0.24	0.76
276.1	3.03	3.23	I	0.10	0.90	0.24	0.76	0.18	0.82
276.1	2.32	2.43	I	0.41	0.60	0.64	0.36	0.57	0.43
276.1	2.50	2.70	I	0.32	0.69	0.40	0.60	0.48	0.52
276.1	2.69	2.88	I	0.23	0.77	0.31	0.69	0.38	0.62
276.1	1.99	2.14	I	0.67	0.33	0.88	0.12	0.80	0.20
276.1	2.17	2.26	I	0.58	0.42	0.78	0.22	0.73	0.27
278.1	3.42	3.64	I	0.20	0.80	0.23	0.77	0.33	0.67
278.1	3.63	3.83	I	0.14	0.86	0.23	0.78	0.24	0.76
278.1	3.80	3.95	I	0.10	0.90	0.15	0.85	0.19	0.81
278.1	3.04	3.33	I	0.32	0.68	0.46	0.54	0.48	0.52
278.1	3.32	3.55	I	0.23	0.77	0.27	0.73	0.37	0.63
278.1	2.58	2.77	I	0.61	0.39	0.79	0.21	0.74	0.26
279.2	3.57	4.09	I	0.20	0.80	0.27	0.73	0.33	0.67
280.2	4.49	4.76	I	0.15	0.85	0.31	0.69	0.25	0.75
280.2	4.66	4.90	I	0.11	0.89	0.25	0.76	0.19	0.81
280.2	3.54	4.14	I	0.34	0.66	0.73	0.27	0.49	0.51
280.2	4.11	4.46	I	0.24	0.77	0.34	0.66	0.37	0.63

280.2	3.14	3.53	I	0.62	0.38	0.86	0.14	0.74	0.26	
280.2	3.48	3.75	I	0.49	0.51	0.79	0.21	0.64	0.36	
282.2	5.77	6.08	I	0.11	0.89	0.28	0.72	0.19	0.81	
284.2	7.19	7.65	I	0.12	0.89	0.11	0.89	0.18	0.82	
AADp		7.8%	AADc					0.07		

279



280

281 **Figure 5. Hydrate composition for methane-carbon dioxide hydrates. Experimental data [68] and simulation**  
 282 **results (sI).**

283 Belandria et al. also studied the hydrate composition of carbon dioxide-nitrogen mixture using  
 284 the same method [65,69]. They calculated the guest composition in gas, liquid and hydrate phases  
 285 based on the material balance and volumetric properties evaluated from equation of state. Table 9  
 286 details their experimental data and our simulation results. Moreover, Figure 6 illustrates the  
 287 experimental [69] and simulation results for two isotherms of N<sub>2</sub>/CO<sub>2</sub> binary hydrates.

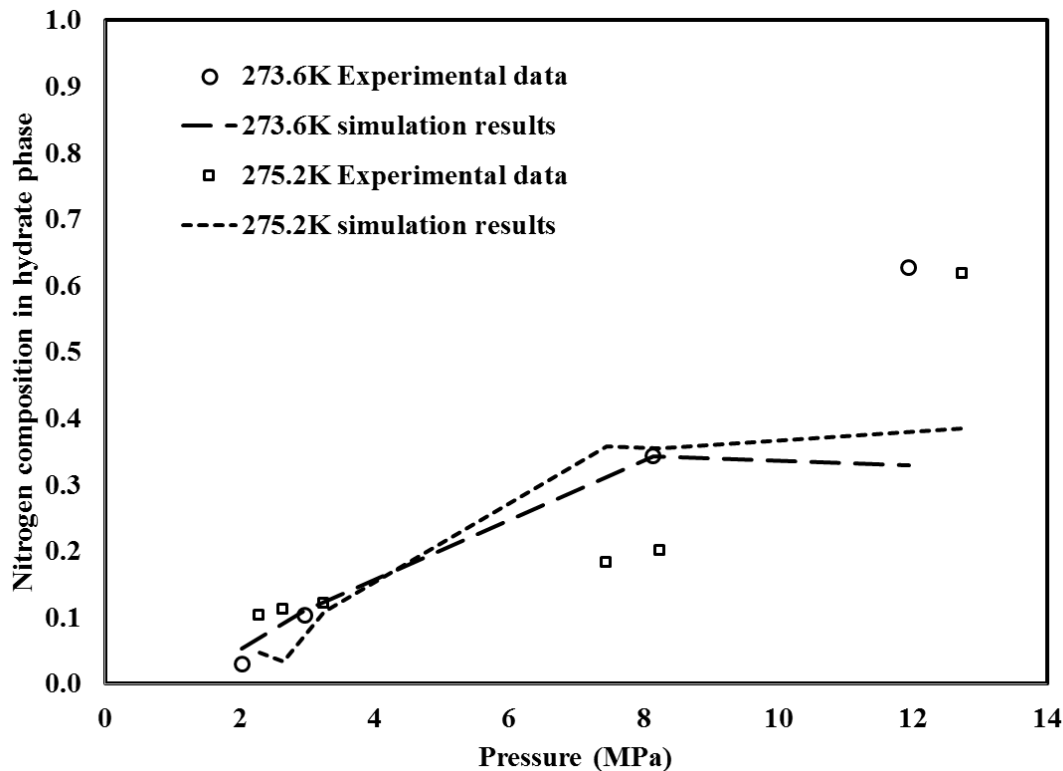
288 **Table 9. Experimental results of Belandria et al. [69] for nitrogen-carbon dioxide mixture hydrates and**  
 289 **simulation results.**

T (K) (±0.02)	P <sub>exp</sub> (MPa) (±0.002)	P <sub>pre</sub> (MPa)	S	Gas composition (exp)		Hydrate composition (exp) (±1%)		Hydrate composition (pre)	
				CO <sub>2</sub>	N <sub>2</sub>	CO <sub>2</sub>	N <sub>2</sub>	CO <sub>2</sub>	N <sub>2</sub>
273.6	2.03	2.22	I	0.62	0.38	0.97	0.03	0.95	0.05

273.6	8.15	7.22	I	0.17	0.83	0.66	0.34	0.66	0.34
273.6	11.94	6.94	I	0.18	0.82	0.37	0.63	0.67	0.33
273.6	2.96	3.17	I	0.43	0.57	0.90	0.10	0.89	0.11
274.6	2.54	2.10	I	0.73	0.27	0.74	0.26	0.97	0.03
274.9	5.20	2.21	I	0.72	0.28	0.79	0.21	0.96	0.04
275.2	2.29	2.51	I	0.66	0.34	0.90	0.10	0.95	0.05
275.2	2.64	2.25	I	0.73	0.27	0.89	0.11	0.97	0.03
275.2	3.26	3.69	I	0.45	0.55	0.88	0.12	0.89	0.11
275.2	7.45	8.83	I	0.17	0.83	0.82	0.18	0.64	0.36
275.2	8.25	8.74	I	0.18	0.82	0.80	0.20	0.65	0.35
275.2	12.75	9.32	I	0.16	0.84	0.38	0.62	0.62	0.38
275.6	2.71	2.36	I	0.73	0.27	0.76	0.24	0.97	0.03
275.8	5.38	2.45	I	0.72	0.28	0.80	0.20	0.96	0.04
276.1	2.50	2.69	I	0.68	0.32	0.98	0.02	0.96	0.04
276.1	2.87	2.50	I	0.73	0.27	0.79	0.21	0.97	0.03
276.1	3.70	3.80	I	0.49	0.51	0.70	0.30	0.90	0.10
276.1	4.40	4.70	I	0.40	0.60	0.69	0.31	0.86	0.14
276.1	8.58	9.07	I	0.20	0.80	0.57	0.43	0.67	0.33
276.7	3.70	4.11	I	0.49	0.51	0.70	0.30	0.90	0.10
277.1	2.71	2.94	I	0.71	0.30	0.84	0.16	0.96	0.04
277.3	3.13	2.89	I	0.73	0.27	0.83	0.17	0.96	0.04
277.8	6.16	3.01	I	0.75	0.25	0.86	0.14	0.97	0.03
278.1	2.97	3.21	I	0.73	0.27	0.89	0.11	0.96	0.04
278.1	3.41	3.19	I	0.73	0.27	0.75	0.25	0.96	0.04
278.1	4.19	4.63	I	0.52	0.48	0.66	0.35	0.91	0.09
278.1	9.15	10.69	I	0.23	0.77	0.54	0.46	0.69	0.31
278.1	14.26	16.69	I	0.13	0.87	0.51	0.49	0.49	0.51
279.7	4.82	5.42	I	0.56	0.44	0.70	0.30	0.91	0.09
279.7	10.02	12.26	I	0.26	0.74	0.61	0.39	0.71	0.29
279.7	15.82	19.25	I	0.15	0.85	0.55	0.45	0.50	0.50
281.2	17.63	21.78	I	0.18	0.82	0.58	0.42	0.53	0.47
281.7	6.33	5.22	I	0.75	0.25	0.81	0.19	0.96	0.04
AADp		17.4%	AADc					0.13	

290

291 From Table 9 and Figure 6, notice that neither equilibrium pressure nor hydrate composition were  
292 well simulated. Nevertheless, at equilibrium pressures below 7MPa, the simulation results were  
293 satisfactory. In contrast, equilibrium pressures more than 7MPa were poorly simulated. In the  
294 case of hydrate composition, the average deviation was large (0.13) compared to the simulation  
295 of experimental data of Kang et al. (0.04) for the same mixture. This divergence might be due to  
296 different experimental procedures.

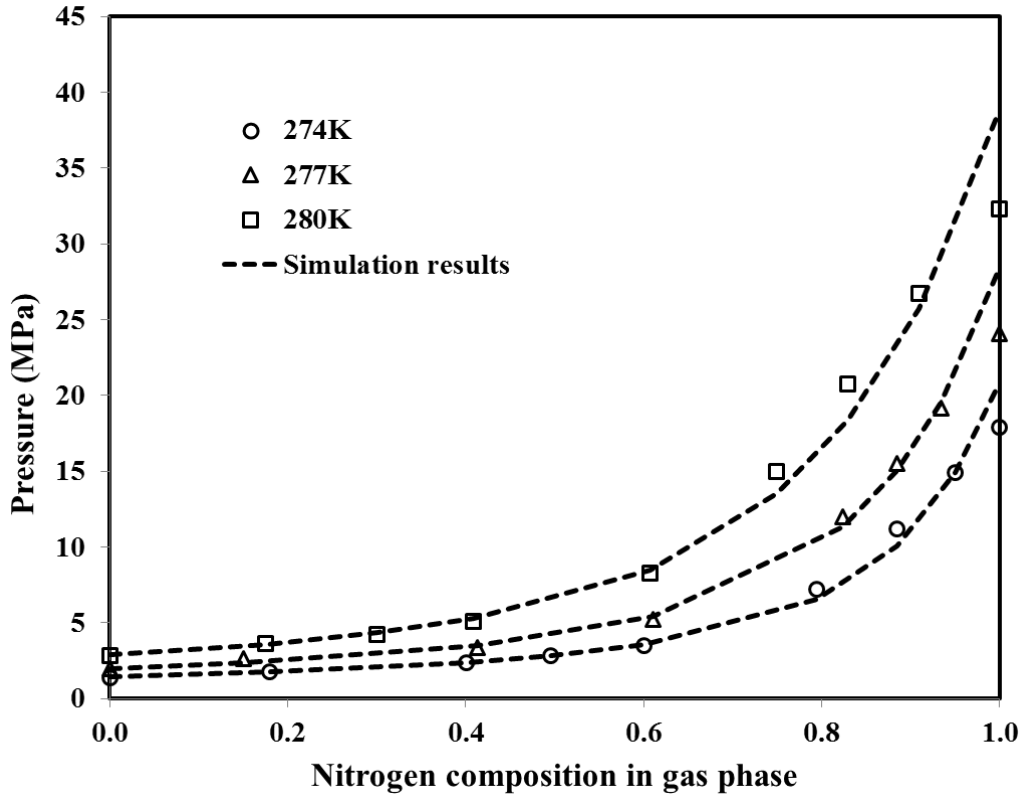


297  
 298 **Figure 6. Hydrate composition for nitrogen-carbon dioxide hydrates at two isotherms. Experimental data [69]**  
 299 **and simulation results (sI).**

300

### 301 **4.3. Gas uptake at isobaric equilibrium condition**

302 Seo et al. studied the vapor-liquid-hydrate equilibrium conditions of nitrogen-carbon dioxide and  
 303 methane-carbon dioxide mixtures at isobaric condition [70]. They performed their experiments in  
 304 a batch reactor by injecting gas mixtures and water by a syringe pump at a desired pressure. Then  
 305 they decreased the temperature to 5 degrees Kelvin below the hydrate formation temperature.  
 306 Hydrate formation led to a decrease in hydrate pressure. In order to keep constant the pressure,  
 307 they recharged reactor by the gas mixtures. Then, they increased the temperature by the rate of 1-  
 308 2 K per hour. The pressure increased due to hydrate dissociation. Then, the dissociated gases  
 309 were vented. When only a small amount of hydrate crystals remained in the cell and the pressure  
 310 was constant, this was considered as the three phase equilibrium [70]. Both their experimental  
 311 and our simulation results for nitrogen-carbon dioxide mixture are listed and presented in Table  
 312 10 and Figure 7. Moreover, the results of methane-carbon dioxide mixture are presented in Table  
 313 11.



314

315 **Figure 7. Pressure-gas composition diagram for nitrogen-carbon dioxide at three isotherms (sI). Experimental**  
 316 **data from Seo et al. [70] and our prediction results**

317 **Table 10. Experimental results of carbon dioxide-nitrogen hydrate equilibrium pressure and composition**  
 318 **from Seo et al. [70] and our simulation results. Composition uncertainties were not provided.**

T (K) (±0.1)	P <sub>exp</sub> (MPa) (±0.01)	P <sub>pre</sub> (MPa)	S	Gas composition (exp)		Hydrate composition (exp)		Hydrate composition (pre)	
				CO <sub>2</sub>	N <sub>2</sub>	CO <sub>2</sub>	N <sub>2</sub>	CO <sub>2</sub>	N <sub>2</sub>
274	1.39	1.42	I	1.00	0.00	1.00	0.00	1.00	0.00
274	1.77	1.74	I	0.82	0.18	0.99	0.02	0.98	0.02
274	2.35	2.39	I	0.60	0.40	0.95	0.05	0.94	0.06
274	2.84	2.84	I	0.50	0.50	0.93	0.07	0.92	0.08
274	3.46	3.57	I	0.40	0.60	0.90	0.10	0.87	0.13
274	7.24	6.55	I	0.21	0.79	0.58	0.42	0.71	0.29
274	11.20	10.03	I	0.12	0.88	0.34	0.66	0.53	0.47
274	14.93	14.91	I	0.05	0.95	0.18	0.82	0.28	0.72
274	17.93	20.81	I	0.00	1.00	0.00	1.00	0.00	1.00
277	1.95	1.99	I	1.00	0.00	1.00	0.00	1.00	0.00
277	2.60	2.38	I	0.85	0.15	0.98	0.02	0.98	0.02
277	3.38	3.52	I	0.59	0.41	0.95	0.05	0.93	0.07
277	5.23	5.40	I	0.39	0.61	0.89	0.11	0.85	0.15
277	11.98	11.30	I	0.18	0.82	0.54	0.46	0.62	0.38

277	15.50	15.07	I	0.12	0.88	0.35	0.65	0.48	0.52	
277	19.17	19.56	I	0.07	0.93	0.19	0.81	0.31	0.69	
277	24.04	28.37	I	0.00	1.00	0.00	1.00	0.00	1.00	
280	2.80	2.86	I	1.00	0.00	1.00	0.00	1.00	0.00	
280	3.60	3.59	I	0.83	0.18	0.98	0.02	0.98	0.02	
280	4.23	4.35	I	0.70	0.30	0.96	0.04	0.95	0.05	
280	5.07	5.29	I	0.59	0.41	0.94	0.06	0.92	0.08	
280	8.28	8.50	I	0.39	0.61	0.86	0.14	0.83	0.17	
280	14.97	13.50	I	0.25	0.75	0.64	0.36	0.68	0.32	
280	20.75	18.39	I	0.17	0.83	0.45	0.55	0.55	0.45	
280	26.69	25.74	I	0.09	0.91	0.22	0.78	0.35	0.65	
280	32.31	38.81	I	0.00	1.00	0.00	1.00	0.00	1.00	
AADp		5.7%	AADc					0.04		

319

320 **Table 11. Experimental results of carbon dioxide-methane hydrate equilibrium pressure and composition**  
321 **from Seo et al. [70] and our simulation results. Composition uncertainties were not provided.**

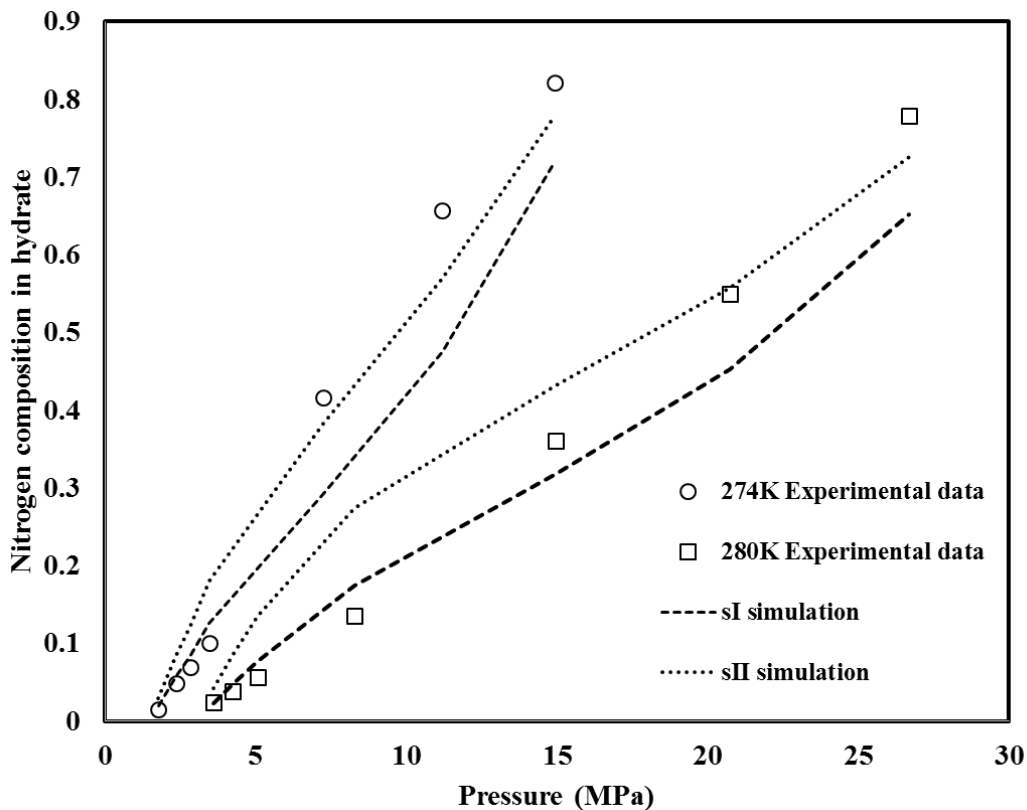
T (K) (±0.1)	P <sub>exp</sub> (MPa) (±0.01)	P <sub>pre</sub> (MPa)	S	Gas composition (exp)		Hydrate composition (exp)		Hydrate composition (pre)		
				CO <sub>2</sub>	CH <sub>4</sub>	CO <sub>2</sub>	CH <sub>4</sub>	CO <sub>2</sub>	CH <sub>4</sub>	
273.1	2.00	1.92	I	0.28	0.72	0.92	0.09	0.45	0.55	
274.1	2.00	2.03	I	0.40	0.60	0.94	0.06	0.58	0.42	
275.4	2.00	2.06	I	0.61	0.39	0.98	0.02	0.75	0.25	
276.3	2.00	2.04	I	0.79	0.21	1.00	0.00	0.88	0.12	
273.8	2.60	2.48	I	0.13	0.87	0.66	0.34	0.24	0.76	
274.9	2.60	2.54	I	0.23	0.77	0.85	0.15	0.38	0.62	
276.3	2.60	2.56	I	0.42	0.59	0.93	0.07	0.58	0.42	
277.5	2.60	2.55	I	0.64	0.36	0.98	0.02	0.77	0.23	
278.1	2.60	2.46	I	0.83	0.17	0.99	0.01	0.90	0.10	
276.6	3.50	3.29	I	0.13	0.87	0.65	0.35	0.24	0.76	
277.6	3.50	3.32	I	0.25	0.75	0.73	0.27	0.40	0.60	
279.0	3.50	3.45	I	0.42	0.58	0.89	0.11	0.57	0.43	
279.9	3.50	3.43	I	0.61	0.39	0.95	0.05	0.74	0.26	
280.5	3.50	3.30	I	0.83	0.17	0.99	0.01	0.90	0.10	
AAD		3.3%						0.29		

322

323 As it is clear in Table 10, Table 11 and Figure 7, the thermodynamic model predicts the  
324 equilibrium pressure with adequate deviations (average deviations for methane-carbon dioxide  
325 and nitrogen-carbon dioxide hydrate pressure were 3.3 and 5.7%, respectively).

326 As seen in Table 10, at low concentrations of nitrogen, the hydrate phase compositions were  
327 acceptably simulated (sI). Nevertheless, when nitrogen was the dominate component in hydrate

328 phase, the simulation results deviated from the experimental data. Hence, the hydrate phase  
 329 compositions were again simulated by taking into account both structures, sI and sII. Prediction  
 330 results for two isotherms of N<sub>2</sub>/CO<sub>2</sub> binary hydrate are presented in Figure 8. This figure shows  
 331 that, at higher pressures, the hydrate preferentially encapsulates nitrogen from the N<sub>2</sub>/CO<sub>2</sub>  
 332 mixture. Consequently, the nitrogen composition in hydrate phase increases. As clear on the  
 333 figure, at high concentrations of nitrogen in hydrate phase, sII simulation results are in better  
 334 agreement with experimental data compared to sI results. This can be explained by the fact that  
 335 pure nitrogen forms sII hydrates. Thus, when nitrogen is the major component in the mixture,  
 336 there might be a structural transition from sI to sII.



337

338 **Figure 8. P-x diagram of N<sub>2</sub>-CO<sub>2</sub> hydrate based on the experimental results of Seo et al. (sI) [70] and our**  
 339 **simulation results**

340 For the methane-carbon dioxide mixture, although the equilibrium pressure were satisfactorily  
 341 simulated (average absolute deviation 3.3%), the thermodynamic model failed to evaluate the  
 342 hydrate composition (average absolute deviation 0.29 mole fraction).

#### 343 4.4. Using a tracer

344 Using a tracer in gas or liquid phase could help to measure hydrate composition. A tracer must  
 345 not be able to form hydrates and only a small amount should be utilized. This section presents a  
 346 short report of publications which have used a tracer in their experiment to measure hydrate

347 composition. Of course, based on the experimental results of these papers, the capability of the  
 348 thermodynamic model to simulate hydrate composition is evaluated.

349 Ng determined the hydrate composition for six gas mixture including methane, ethane, propane,  
 350 iso-butane, n-butane and carbon dioxide. He used n-pentane as a tracer in gas phase. Thanks to a  
 351 gasometer and composition of n-pentane at the end of experiments, he successfully determined  
 352 the amount of original gas mixture and overall gas dissociation [71]. Table 12 shows the different  
 353 gas mixtures in the study. Ng's experimental data and our simulation results are presented in  
 354 Table 13.

355 **Table 12. Feed composition of different mixtures [71]**

Gas	Mixtures (Concentration mole %) ( $\pm 0.003$ )					
	a	b	c	d	e	f
Carbon dioxide	0	0	0	2	0	2
Methane	90	99	84	88	80	86.5
Ethane	0	0	10	0	10	0
Propane	10	1	4	8	5	4
iso-Butane	0	0	2	2	2	0.5
n-Butane	0	0	0	0	3	1

356

357 **Table 13. Experimental results of Ng [71] and our modeling results**

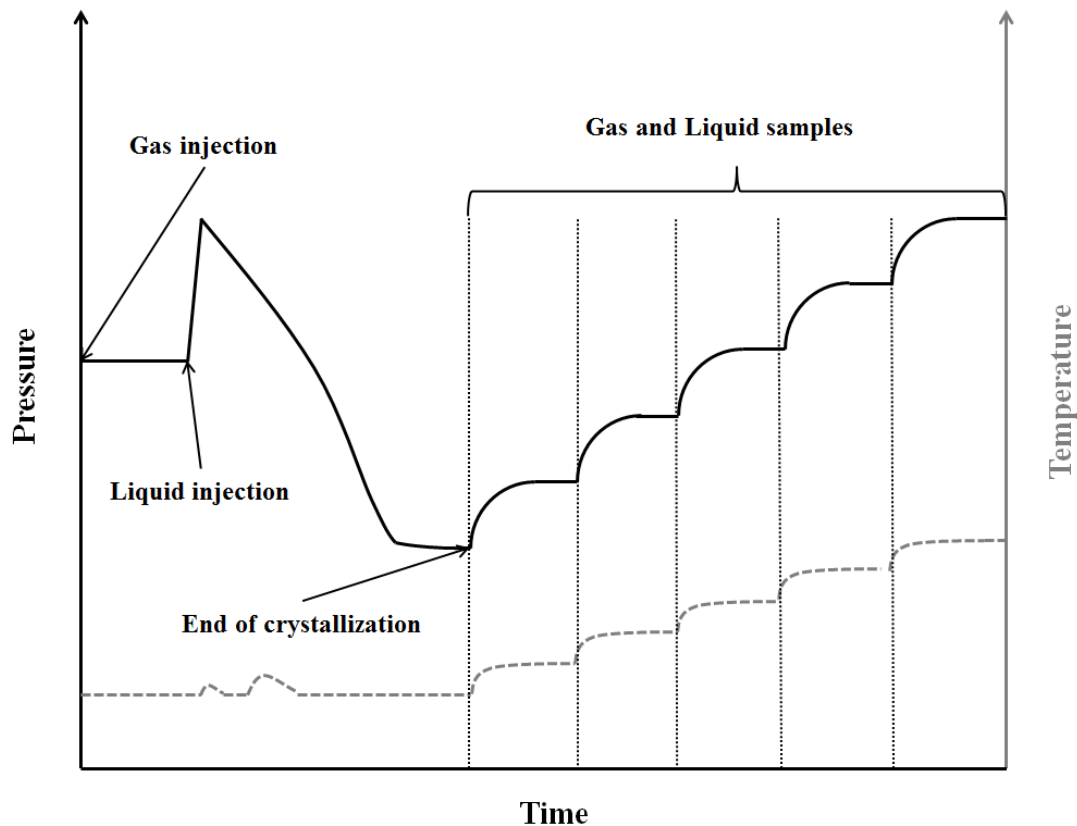
T (C) ( $\pm 0.05$ )	P (MPa) ( $\pm 0.007$ )	Feed	Experimental hydrate composition ( $\pm 0.003$ )						Hydrate composition simulation					
			C <sub>1</sub>	C <sub>2</sub>	C <sub>3</sub>	iC <sub>4</sub>	nC <sub>4</sub>	CO <sub>2</sub>	C <sub>1</sub>	C <sub>2</sub>	C <sub>3</sub>	iC <sub>4</sub>	nC <sub>4</sub>	CO <sub>2</sub>
11.4	2.07	a	0.586	-	0.414	-	-	-	0.61	-	0.39	-	-	-
20.1	6.89	a	0.657	-	0.343	-	-	-	0.64	-	0.36	-	-	-
3.7	2.07	b	0.726	-	0.274	-	-	-	0.65	-	0.35	-	-	-
13.2	6.89	b	0.771	-	0.229	-	-	-	0.67	-	0.33	-	-	-
AADc									0.05					
10.9	2.07	c	0.606	0.087	0.182	0.124	-	-	0.62	0.01	0.2	0.17	-	-
19.4	6.89	c	0.59	0.087	0.2	0.123	-	-	0.64	0.01	0.2	0.15	-	-
AADc									0.03	0.07	0.009	0.02		
12.9	2.07	d	0.6	-	0.297	0.092	-	0.0102	0.6	-	0.28	0.1	-	0.02
21.6	6.89	d	0.63	-	0.289	0.078	-	0.0104	0.62	-	0.27	0.09	-	0.02
AADc									0.005	-	0.018	0.01	-	0.01
11.3	2.07	e	0.581	0.074	0.206	0.107	0.031	-	0.62	0.01	0.22	0.14	0.01	-
19.6	6.89	e	0.617	0.089	0.181	0.087	0.027	-	0.64	0.01	0.23	0.11	0.01	-
AADc									0.031	0.07	0.03	0.02	0.02	
9.8	2.07	f	0.584	0.076	0.265	0.044	0.018	0.011	0.6	0.006	0.31	0.06	0.007	0.017
18.7	6.89	f	0.621	0.077	0.238	0.039	0.011	0.01	0.63	0.007	0.29	0.05	0.006	0.017
AADc									0.01	0.07	0.05	0.01	0.008	0.006

358

359 Obviously, in Table 13, there is a wide range of average absolute deviation according to the  
 360 number and type of components in the feed gas, between 0.006 and 0.07. This variation could be

361 explained by the fact that for the ternary or quaternary mixtures, kinetic considerations might  
362 affect experimental results. Note: the largest deviation belongs to ethane in all the mixtures.

363 In the 21st century, researchers at Ecole National Supérieur des Mines de Saint-Etienne (Mines  
364 Saint-Etienne) developed a new method to determine the hydrate composition not only at  
365 equilibrium condition, but also during the crystallization under non-equilibrium conditions. Their  
366 new procedure was based on tracing the concentration of lithium salt in liquid phase and material  
367 balance. The protocol is as follows: after gas injection inside the reactor, water solution with 10  
368 ppm concentration of lithium salt was inserted in the reactor. By decreasing the temperature at a  
369 desired value, hydrate formation started. After several days, the system reached at equilibrium. At  
370 this point a gas and liquid sample was taken. The gas sample was analyzed by gas  
371 chromatography to determine the gas composition in vapor phase. The liquid sample was  
372 analyzed by ion chromatograph to measure the concentration of lithium salt in liquid phase. As  
373 lithium does not participate in hydrate formation, it is possible to calculate the amount of water at  
374 equilibrium according to the lithium concentration. Then, the system temperature increased  
375 stepwise and gas and liquid samples were taken [14,57]. A diagram of their experiments is shown  
376 in Figure 9.



377

378

**Figure 9. The diagram of experimental procedure**

379 Based on this procedure, Herri et al. [14] studied the equilibrium conditions of carbon dioxide-  
380 nitrogen and carbon dioxide-methane hydrates. Table 14 and Table 15 present their experimental

381 results and our corresponding simulation results for carbon dioxide-nitrogen and carbon dioxide-  
 382 methane mixtures, respectively.

383 **Table 14. Experimental results from Herri et al. [14] and simulation results for carbon dioxide-nitrogen**  
 384 **mixture**

T (K) (±0.1)	P <sub>exp</sub> (MPa) (±0.01)	P <sub>pre</sub> (MPa)	S	Gas composition (exp) (±0.001)		Hydrate composition (exp) (±0.003)		Hydrate composition (pre)		
				CO <sub>2</sub>	N <sub>2</sub>	CO <sub>2</sub>	N <sub>2</sub>	CO <sub>2</sub>	N <sub>2</sub>	
273.4	6.10	7.51	I	0.16	0.84	0.66	0.34	0.63	0.37	
274.5	6.20	8.31	I	0.16	0.84	0.66	0.34	0.63	0.37	
275.4	6.40	8.64	I	0.19	0.82	0.66	0.34	0.66	0.34	
276.5	6.60	9.42	I	0.20	0.80	0.58	0.42	0.67	0.33	
273.9	5.90	5.40	I	0.25	0.75	0.75	0.25	0.77	0.23	
274.7	5.90	5.93	I	0.26	0.75	0.73	0.27	0.76	0.24	
276.0	5.90	6.90	I	0.26	0.74	0.70	0.30	0.76	0.24	
276.9	6.00	7.70	I	0.27	0.74	0.70	0.30	0.75	0.25	
277.8	6.30	8.14	I	0.29	0.71	0.67	0.33	0.77	0.23	
278.1	6.40	8.41	I	0.30	0.71	0.69	0.31	0.77	0.23	
278.4	6.40	8.82	I	0.30	0.71	0.72	0.29	0.76	0.24	
278.6	6.50	8.93	I	0.30	0.70	0.70	0.31	0.77	0.23	
275.4	6.10	7.99	I	0.20	0.80	0.67	0.33	0.69	0.31	
276.0	6.20	8.14	I	0.22	0.78	0.65	0.35	0.70	0.30	
280.1	5.30	5.75	I	0.56	0.44	0.85	0.16	0.91	0.09	
281.1	5.60	6.42	I	0.59	0.42	0.82	0.18	0.91	0.09	
AADp		25.6%	AADc				0.05			

385

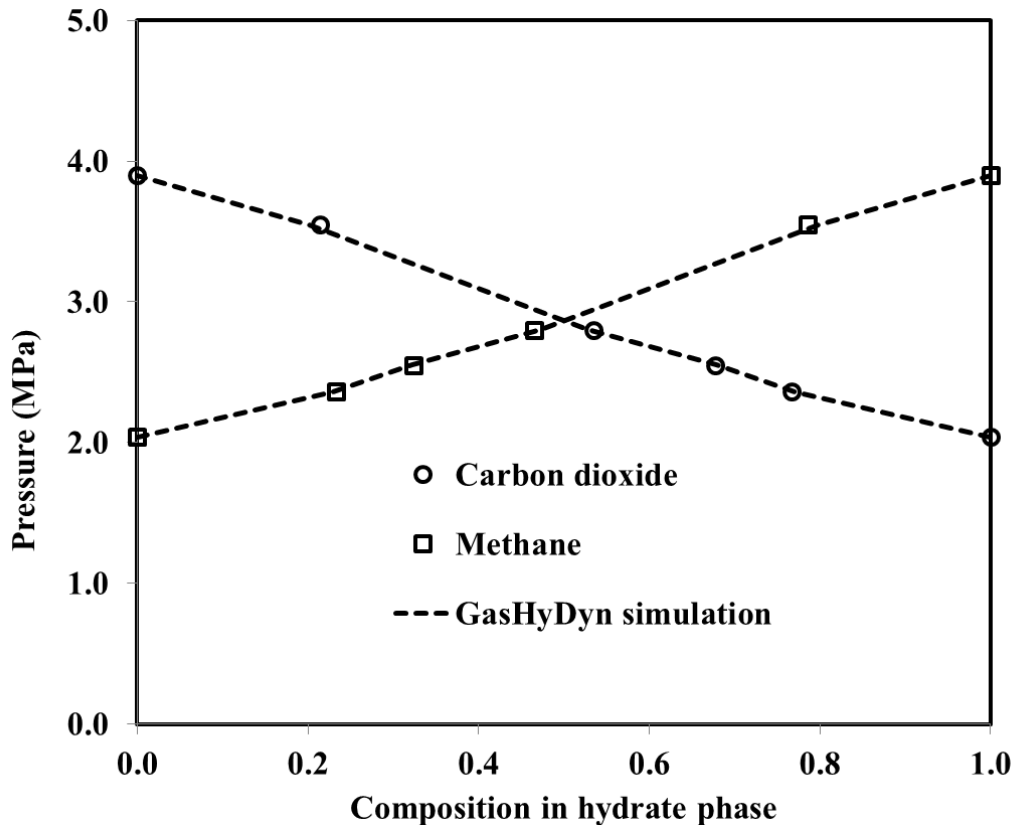
386 **Table 15. Experimental results from Herri et al. [14] and simulation results for carbon dioxide-methane**  
 387 **mixture**

T (K) (±0.1)	P <sub>exp</sub> (MPa) (±0.01)	P <sub>pre</sub> (MPa)	S	Gas composition (exp) (±0.001)		Hydrate composition (exp) (±0.003)		Hydrate composition (pre)		
				CO <sub>2</sub>	CH <sub>4</sub>	CO <sub>2</sub>	CH <sub>4</sub>	CO <sub>2</sub>	CH <sub>4</sub>	
277.15	2.04	2.03	I	1.00	0.00	1.00	0.00	1.00	0.00	
277.15	2.36	2.45	I	0.64	0.36	0.77	0.23	0.77	0.23	
277.15	2.55	2.63	I	0.52	0.48	0.68	0.32	0.68	0.32	
277.15	2.80	2.92	I	0.36	0.64	0.54	0.47	0.53	0.47	
277.15	3.55	3.55	I	0.11	0.89	0.21	0.79	0.20	0.80	
277.15	3.90	3.94	I	0.00	1.00	0.00	1.00	0.00	1.00	
AADp		2.10%	AADc				0.004			

388

389 In the case of carbon dioxide-nitrogen, the simulation results for hydrate equilibrium pressure are  
 390 not very reliable. Nonetheless, the average absolute deviation for prediction of hydrate

391 composition is small (0.05). For carbon dioxide-methane mixture, the simulation results are in  
 392 respectable agreement with the experimental results. As it can be seen in Table 15, the average  
 393 deviation of equilibrium pressure was about 2%. The thermodynamic model better predicts the  
 394 hydrate composition. The average deviation for carbon dioxide and methane compositions in  
 395 hydrate phase was 0.004. Figure 10 presents clearly the excellent match between the  
 396 experimental and simulation results for carbon dioxide-methane hydrate mixture.



397  
 398 **Figure 10. Experimental data from Herri et al. [14] for methane-carbon dioxide hydrate (sI) and simulation**  
 399 **results**

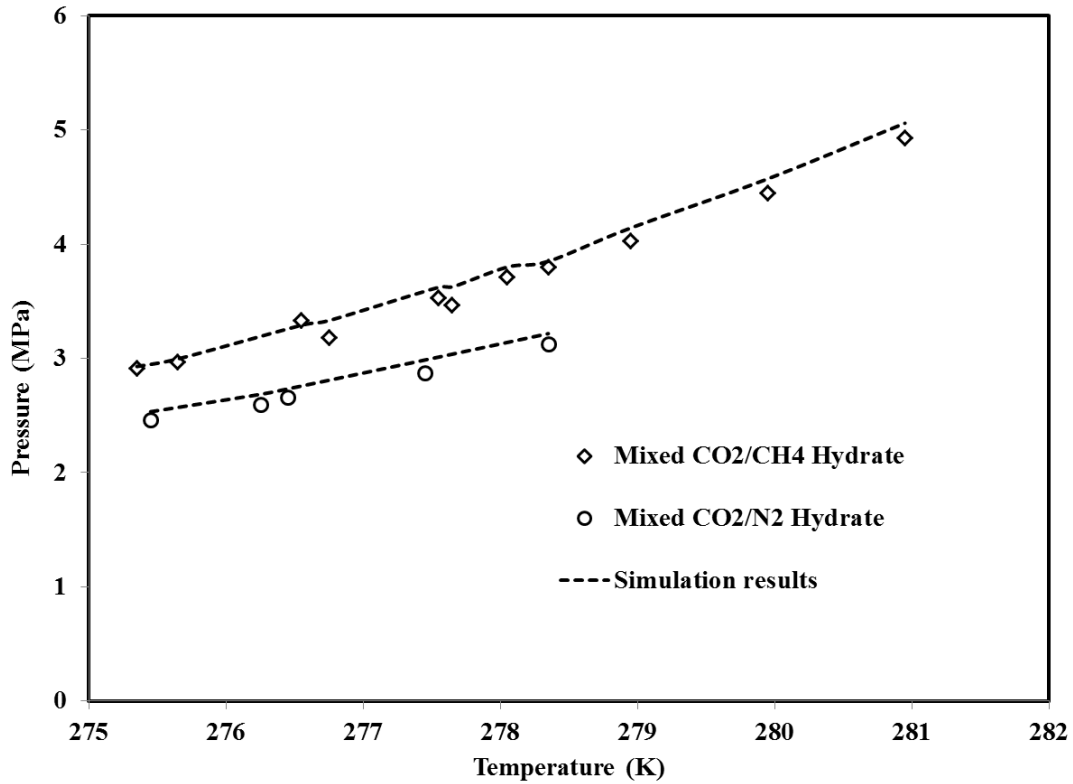
400 Le Quang et al. studied the equilibrium conditions of several gas mixtures from  $N_2$ - $CO_2$ - $CH_4$ -  
 401  $C_2H_6$ - $C_3H_8$ - $nC_4H_{10}$ . They also determined the guest composition in vapor and hydrate phases  
 402 [57]. They used the same method as Herri et al [14] to analyze guest composition in different  
 403 phases. In addition, they studied the influence of crystallization rate on the final equilibrium  
 404 pressure and composition during the crystallization of  $CO_2$ - $CH_4$ - $C_2H_6$  mixed hydrate. All the  
 405 experimental data and our equivalent simulation results are listed in Table 16, Table 17 and Table  
 406 18. They reported that, for the equilibrium points near total dissociation, hydrate composition was  
 407 suspected to have large errors. Thus, they were not used for our purposes. As Table 16 shows, the  
 408 thermodynamic model realistically predicts the equilibrium pressures of binary mixtures  
 409 including carbon dioxide. The average deviation of the equilibrium pressure predictions for  $CO_2$ -

410 CH<sub>4</sub> and CO<sub>2</sub>-N<sub>2</sub> are about 2 and 3%, respectively. For hydrate composition extrapolation, the  
 411 average absolute deviations are 0.05 and 0.04 for CO<sub>2</sub>-CH<sub>4</sub> and CO<sub>2</sub>-N<sub>2</sub>, respectively.

412 **Table 16. Carbon dioxide-methane and carbon dioxide-nitrogen hydrate mixtures, experimental data [57] and**  
 413 **simulation results**

Gas	T <sub>exp</sub> (°C) (±0.1)	P <sub>exp</sub> (MPa) (±0.01)	P <sub>pre</sub> (MPa)	S	Gas composition (exp) (±0.001)			Hydrate composition (exp) (±0.003)			Hydrate composition (Pre)		
					N <sub>2</sub>	CO <sub>2</sub>	CH <sub>4</sub>	N <sub>2</sub>	CO <sub>2</sub>	CH <sub>4</sub>	N <sub>2</sub>	CO <sub>2</sub>	CH <sub>4</sub>
CO <sub>2</sub> -CH <sub>4</sub>	3.4	3.33	3.29	I	-	0.13	0.87	-	0.32	0.68	-	0.23	0.77
	4.4	3.53	3.62	I	-	0.13	0.87	-	0.32	0.68	-	0.24	0.76
	4.9	3.71	3.80	I	-	0.14	0.86	-	0.32	0.68	-	0.24	0.76
	5.8	4.03	4.14	I	-	0.15	0.85	-	0.32	0.68	-	0.26	0.74
	6.8	4.45	4.57	I	-	0.16	0.84	-	0.32	0.68	-	0.27	0.73
	7.8	4.93	5.06	I	-	0.18	0.83	-	0.30	0.70	-	0.28	0.72
	2.2	2.91	2.93	I	-	0.12	0.88	-	0.29	0.71	-	0.22	0.78
	2.5	2.97	3.00	I	-	0.13	0.87	-	0.28	0.72	-	0.23	0.77
	3.6	3.18	3.33	I	-	0.14	0.87	-	0.28	0.72	-	0.24	0.76
	4.5	3.47	3.63	I	-	0.15	0.85	-	0.27	0.73	-	0.25	0.75
	5.2	3.80	3.85	I	-	0.16	0.84	-	0.23	0.77	-	0.27	0.73
AADp		2.4%		AADc						0.05			
CO <sub>2</sub> -N <sub>2</sub>	2.3	2.46	2.53	I	0.33	0.67	-	0.06	0.94	-	0.05	0.95	-
	3.1	2.60	2.69	I	0.31	0.69	-	0.07	0.93	-	0.04	0.96	-
	3.3	2.66	2.73	I	0.30	0.70	-	0.07	0.93	-	0.04	0.96	-
	4.3	2.87	2.99	I	0.28	0.72	-	0.09	0.91	-	0.04	0.96	-
	5.2	3.13	3.22	I	0.25	0.75	-	0.12	0.88	-	0.03	0.97	-
	AADp		3.16%		AADc						0.04		

414



415

416 **Figure 11. P-T diagram of mixed CO<sub>2</sub>/CH<sub>4</sub> and CO<sub>2</sub>/N<sub>2</sub> hydrates, experimental data [57] and simulation**  
 417 **results (sI). The vapor and hydrate compositions were listed in Table 16.**

418

419 As aforementioned, Le Quang et al. investigated the effect of crystallization rate on hydrate  
 420 equilibrium pressure and composition of CO<sub>2</sub>-CH<sub>4</sub>-C<sub>2</sub>H<sub>6</sub> ternary mixture. They reported that the  
 421 hydrate equilibrium pressure and composition at final state differed according to the rate of  
 422 crystallization. They concluded that at quick crystallization rate, mixed gas hydrate could not be  
 423 at thermodynamic equilibrium [57]. Table 17 reveals that the results of thermodynamic model is  
 424 closer to the slow crystallization data. The average deviations of equilibrium pressure prediction  
 425 for slow and quick crystallization are about 2 and 8%, respectively. The average deviations for  
 426 carbon dioxide in hydrate phase for slow and quick crystallization are similar (0.01). This is not  
 427 the case for methane and ethane compositions in hydrate phase, where the deviation of simulation  
 428 for slow crystallization are much better compared to quick rate (e.g. ethane, 0.009 for slow  
 429 compared to 0.05 for quick).

430

431

432

433  
434

**Table 17. Experimental results of Carbon dioxide-methane-ethane hydrate from Le Quang et al. [57] and simulation results**

Gas	T <sub>exp</sub> (°C) (±0.1)	P <sub>exp</sub> (MPa) (±0.01)	P <sub>pre</sub> (MPa)	S	Gas composition (exp) (±0.001)			Hydrate composition (exp) (±0.003)			Hydrate composition (Pre)		
					CO <sub>2</sub>	CH <sub>4</sub>	C <sub>2</sub> H <sub>6</sub>	CO <sub>2</sub>	CH <sub>4</sub>	C <sub>2</sub> H <sub>6</sub>	CO <sub>2</sub>	CH <sub>4</sub>	C <sub>2</sub> H <sub>6</sub>
CO <sub>2</sub> -CH <sub>4</sub> -C <sub>2</sub> H <sub>6</sub> Quick crys.	2.75	3.54	3.11	I	0.03	0.96	0.01	0.07	0.89	0.04	0.05	0.87	0.08
	3.65	3.81	3.35	I	0.03	0.96	0.01	0.07	0.89	0.04	0.05	0.86	0.09
	5.15	4.23	3.79	I	0.03	0.95	0.02	0.07	0.89	0.04	0.05	0.83	0.11
	6.55	4.56	4.33	I	0.03	0.95	0.02	0.07	0.89	0.04	0.06	0.83	0.12
	7.80	5.12	4.76	I	0.04	0.94	0.02	0.07	0.89	0.04	0.06	0.81	0.13
	9.25	5.99	5.67	I	0.04	0.94	0.02	0.04	0.90	0.07	0.07	0.82	0.12
	AADp		8.6%		AADc						0.01	0.05	0.05
CO <sub>2</sub> -CH <sub>4</sub> -C <sub>2</sub> H <sub>6</sub> Slow crys.	4.60	3.78	3.64	I	0.04	0.95	0.01	0.08	0.80	0.12	0.06	0.84	0.09
	4.20	3.56	3.50	I	0.03	0.95	0.01	0.08	0.83	0.09	0.06	0.84	0.10
	3.25	3.18	3.27	I	0.03	0.96	0.01	0.08	0.85	0.08	0.06	0.87	0.07
	1.30	2.76	2.76	I	0.03	0.96	0.01	0.08	0.86	0.06	0.06	0.89	0.05
	4.20	3.57	3.46	I	0.04	0.95	0.02	0.06	0.84	0.09	0.07	0.83	0.10
	AADp		2.2%		AADc						0.01	0.02	0.01

435

436 As seen in Table 18, the average deviation of the equilibrium pressures calculated for the  
437 quaternary mixture of methane-ethane-propane-butane is about 13% which is expected due to  
438 more significant kinetic effects in quaternary mixtures.

439 Hydrate composition for the methane and butane is well simulated (AADc=0.01), while for  
440 ethane and propane, the average deviation of hydrate composition are 0.06 and 0.07, respectively.

441 **Table 18. Experimental data of methane-ethane-propane-butane hydrate from Le Quang et al. [57] and**  
442 **simulation results**

T <sub>exp</sub> (°C) (±0.1)	P <sub>exp</sub> (MPa) (±0.01)	P <sub>pre</sub> (MPa)	S	Gas composition (exp) (±0.001)				Hydrate composition (exp) (±0.003)				Hydrate composition (Pre)			
				C <sub>1</sub>	C <sub>2</sub>	C <sub>3</sub>	C <sub>4</sub>	C <sub>1</sub>	C <sub>2</sub>	C <sub>3</sub>	C <sub>4</sub>	C <sub>1</sub>	C <sub>2</sub>	C <sub>3</sub>	C <sub>4</sub>
2.40	2.28	1.70	II	0.97	0.02	0.00	0.01	0.73	0.11	0.11	0.05	0.75	0.03	0.16	0.06
3.45	2.31	1.82	II	0.97	0.02	0.01	0.01	0.73	0.11	0.11	0.05	0.74	0.03	0.18	0.06
7.60	2.75	2.50	II	0.94	0.04	0.01	0.02	0.71	0.10	0.14	0.05	0.72	0.04	0.18	0.07
9.15	2.97	2.70	II	0.93	0.04	0.01	0.02	0.68	0.10	0.17	0.05	0.70	0.03	0.20	0.06
9.90	3.05	2.78	II	0.92	0.04	0.02	0.02	0.68	0.10	0.17	0.05	0.70	0.03	0.22	0.05
10.80	3.12	2.86	II	0.92	0.05	0.02	0.02	0.69	0.10	0.17	0.05	0.69	0.03	0.24	0.04
11.70	3.22	2.94	II	0.91	0.05	0.03	0.02	0.69	0.10	0.16	0.05	0.68	0.02	0.25	0.04
12.65	3.34	3.09	II	0.90	0.05	0.03	0.02	0.70	0.09	0.16	0.05	0.68	0.02	0.26	0.04
13.65	3.46	3.32	II	0.89	0.05	0.04	0.02	0.70	0.09	0.16	0.05	0.68	0.02	0.27	0.03
14.70	3.48	3.75	II	0.89	0.05	0.04	0.02	0.70	0.09	0.16	0.05	0.68	0.02	0.27	0.03
15.65	3.52	4.20	II	0.89	0.05	0.04	0.02	0.70	0.09	0.16	0.05	0.68	0.02	0.27	0.03

16.60	3.61	4.61	II	0.88	0.05	0.04	0.02	0.71	0.09	0.16	0.05	0.68	0.02	0.27	0.03
2.75	2.14	1.52	II	0.96	0.02	0.01	0.01	0.73	0.08	0.15	0.04	0.71	0.03	0.19	0.07
4.30	2.16	1.80	II	0.96	0.02	0.01	0.01	0.73	0.08	0.15	0.04	0.72	0.03	0.18	0.07
4.85	2.18	1.82	II	0.95	0.03	0.01	0.01	0.73	0.08	0.15	0.04	0.71	0.02	0.21	0.06
5.90	2.21	1.98	II	0.95	0.03	0.01	0.01	0.72	0.08	0.16	0.04	0.71	0.02	0.21	0.06
6.80	2.26	2.14	II	0.95	0.03	0.01	0.01	0.72	0.08	0.16	0.04	0.71	0.02	0.22	0.05
7.45	2.36	2.12	II	0.94	0.03	0.02	0.02	0.72	0.08	0.16	0.04	0.69	0.02	0.24	0.05
9.20	2.53	2.31	II	0.93	0.04	0.02	0.02	0.71	0.08	0.17	0.04	0.68	0.02	0.26	0.04
11.05	2.82	2.55	II	0.91	0.04	0.03	0.02	0.71	0.07	0.18	0.04	0.67	0.02	0.27	0.04
AADp		13%	AADc									0.01	0.06	0.07	0.01

443

#### 444 4.5. Microscopic measurements tools

445 In the previous sections, various indirect methods of determining hydrate composition have been  
 446 reviewed. All approaches were based on measuring fluid and system properties like pressure,  
 447 temperature, gas phase composition etc. and then calculating the hydrate composition according  
 448 to the material balance and hydrate properties. Recently, innovative microscopic instruments  
 449 helped researchers to measure directly the properties and molecular aspects of clathrate hydrates  
 450 such as hydrate structure, cage occupancy, hydrate composition and guest molecule position.

##### 451 4.5.1. Experimental data and simulation results

452 One of the first studies using Raman spectroscopy was performed by Sum et al [72] to explore  
 453 the properties of clathrate hydrates for pure guest molecules such as CH<sub>4</sub>, CO<sub>2</sub>, C<sub>3</sub>H<sub>8</sub> and binary  
 454 mixtures CH<sub>4</sub>-CO<sub>2</sub>, CD<sub>4</sub>-C<sub>3</sub>H<sub>8</sub>, CH<sub>4</sub>-N<sub>2</sub>, CH<sub>4</sub>-THF<sub>d8</sub> and CH<sub>4</sub>-C<sub>7</sub>D<sub>14</sub>. As to hydrate composition,  
 455 they only reported the guest composition in hydrate phase for CH<sub>4</sub>-CO<sub>2</sub> binary mixture. Their  
 456 procedure included several steps; preparation of hydrate sample in cell and setting the cell into  
 457 the sample chamber of the Raman. Then, the pressure was adjusted to a value which was within  
 458 5% of the predicted pressure at a desired temperature. They predicted hydrate equilibrium  
 459 pressure by CSMHYD [60,72]. Spectra were then collected at the equilibrium conditions for  
 460 hydrate composition analyses. Table 19 presents their experimental data and reciprocal  
 461 simulation results by the thermodynamic model.

462

**Table 19. Experimental data from Sum et al. [72] and simulation results**

T (K)	Gas composition (exp)		S	Hydrate composition (exp) (±1%)		Hydrate composition (pre)	
	CO <sub>2</sub>	CH <sub>4</sub>		CO <sub>2</sub>	CH <sub>4</sub>	CO <sub>2</sub>	CH <sub>4</sub>
273.15	0.57	0.43	I	0.75	0.25	0.73	0.27
274.15	0.57	0.43	I	0.73	0.27	0.73	0.27
277.15	0.57	0.43	I	0.71	0.29	0.72	0.28
278.15	0.57	0.43	I	0.71	0.29	0.72	0.28
273.15	0.34	0.66	I	0.55	0.45	0.52	0.48

274.15	0.34	0.66	I	0.55	0.45	0.51	0.49
275.15	0.34	0.66	I	0.53	0.47	0.51	0.49
278.15	0.34	0.66	I	0.52	0.48	0.50	0.50
					AADc	0.02	

463

464 Table 19 illustrates that the thermodynamic model satisfactorily simulated the hydrate  
465 composition. The average absolute deviation for hydrate composition was 0.02.

466 Subramanian et al. studied the structural transition of methane-ethane hydrate mixture based on  
467 Raman spectroscopy and <sup>13</sup>C NMR measurements [73,74]. According to the Raman spectra, they  
468 reported that for methane-ethane hydrate mixture at 274.2 K, there was a structural transition  
469 from structure I to II, when the methane composition in gas phase was between 0.722 and 0.750  
470 (mole fraction). Moreover, they observed that the structure changed from sII to sI, once the  
471 methane composition in vapor phase was between 0.992 and 0.994 (mole fraction). Furthermore,  
472 Raman spectra showed that structural transition leads to a 20% variation in hydrate composition.  
473 They also measured the hydrate composition by <sup>13</sup>C NMR at six different vapor compositions.  
474 Their results are listed in Table 20.

475 **Table 20. Experimental data from Subramanian et al. [74] for methane-ethane mixture and simulation results**

T (K)	P <sub>exp</sub> (MPa) (±0.014)	P <sub>pre</sub> (MPa)	S	Gas composition (exp)		Hydrate composition (exp) (±0.1%)		Hydrate composition (Pre)	
				CH <sub>4</sub>	C <sub>2</sub> H <sub>6</sub>	CH <sub>4</sub>	C <sub>2</sub> H <sub>6</sub>	CH <sub>4</sub>	C <sub>2</sub> H <sub>6</sub>
274.2	0.88	0.82	I	0.63	0.37	0.28	0.72	0.30	0.70
274.2	0.96	0.88	I	0.68	0.32	0.36	0.64	0.32	0.68
274.2	0.97	0.96	I	0.72	0.28	0.37	0.63	0.35	0.65
AADp		5.3%	I	AADc				0.02	
274.2	0.99	1.02	II	0.75	0.25	0.57	0.43	0.37	0.63
274.2	1.17	1.34	II	0.85	0.15	0.65	0.35	0.47	0.53
274.2	1.45	1.76	II	0.92	0.08	0.70	0.30	0.61	0.39
AADp		41.6%	II	AADc				0.09	

476

477 Clearly, in Table 20, the thermodynamic simulation concurs with the experimental results for  
478 structure I. While for the structure II, the simulations fail. This reveals that the thermodynamic  
479 model cannot be proficient to well evaluate the hydrate equilibrium conditions when the structure  
480 transition occurs in the system.

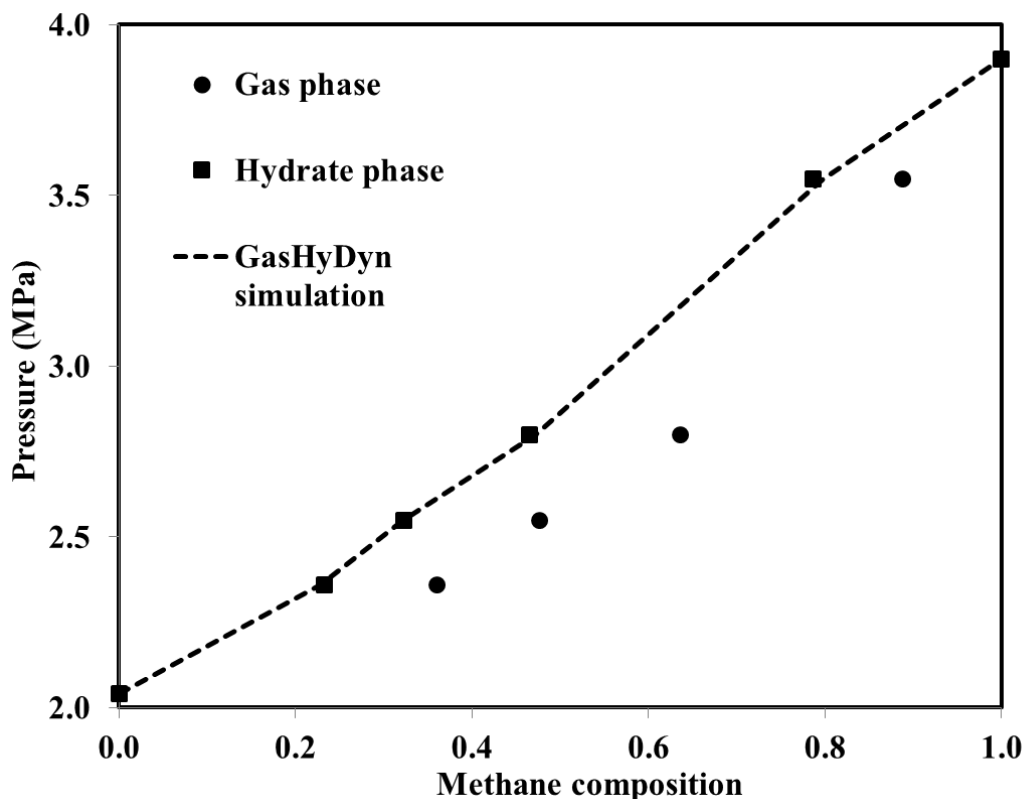
481 Seo and Lee [75] analyzed the structure and gas distribution of nitrogen-carbon dioxide hydrate  
482 at different vapor compositions. They revealed from X-ray diffraction patterns that when carbon  
483 dioxide composition in gas phase was between 3 and 20 mole percent, structure sI formed. While  
484 for CO<sub>2</sub> composition under 1%, the hydrate structure seemed to be sII. Additionally, they  
485 measured the hydrate composition by NMR spectroscopic analyses. They noticed that the CO<sub>2</sub>

486 molecules were mostly localized in the large sI cages. Also, the hydrate composition was  
 487 significantly augmented by a small increase of CO<sub>2</sub> in the vapor phase. Table 21 and Figure 12  
 488 present their experimental and our simulation results for hydrate guest distribution. This is clear  
 489 from the figure that the results of thermodynamic model for hydrate composition prediction  
 490 corresponds well with the experimental data (average deviation of hydrate phase prediction is  
 491 0.02).

492 **Table 21. Experimental results from Seo and Lee [75] and our simulation results**

T (K)	P <sub>exp</sub> (MPa)	P <sub>pre</sub> (MPa)	S	Gas composition (exp)		Hydrate composition (exp) ( $\pm 0.1\%$ )		Hydrate composition (Pre)	
				CO <sub>2</sub>	N <sub>2</sub>	CO <sub>2</sub>	N <sub>2</sub>	CO <sub>2</sub>	N <sub>2</sub>
272.1	14.50	13.57	I	0.01	0.99	0.09	0.91	0.07	0.93
272.1	13.00	12.11	I	0.03	0.97	0.15	0.85	0.17	0.83
272.1	10.50	8.79	I	0.10	0.90	0.47	0.54	0.41	0.59
272.1	7.70	6.24	I	0.18	0.82	0.59	0.41	0.61	0.39
272.1	5.00	3.99	I	0.33	0.67	0.74	0.26	0.79	0.21
272.1	4.10	2.80	I	0.50	0.50	0.86	0.14	0.88	0.12
272.1	3.50	2.14	I	0.67	0.34	0.94	0.06	0.94	0.06
272.1	3.20	1.69	I	0.85	0.15	0.97	0.04	0.98	0.02
AADp		23.3%		AADc				0.02	

493



494

495 **Figure 12. CO<sub>2</sub> composition in gas and hydrate phase versus pressure for CO<sub>2</sub>-N<sub>2</sub> system at 272.1 K (sI).**  
 496 **Experimental [75] and our simulation results**

497 Uchida et al. [76] investigated cage occupancy, hydrate composition and structure of methane-  
 498 ethane mixture by Raman spectroscopy and XRD analyses [76]. They prepared the mixed  
 499 methane-ethane hydrates from ice powder at different feed guest compositions. In the case of  
 500 hydrate structure by Raman spectroscopy, they reported that, when the composition of ethane in  
 501 the gas phase was below 2% or over 22% mole fraction, only structure I exists. However, there  
 502 was a coexistence of both structures I and II at ethane concentrations between 12 and 22% mole  
 503 fraction. Results of XRD analyses confirmed these investigations. They also observed that ethane  
 504 molecules were only encapsulated in large cavities, while the methane molecules occupied both  
 505 small and large cavities. Interestingly, their results revealed that the vapor composition had a  
 506 significant influence on the cage occupancy in large cavities [76].

507 Uchida et al. [77] expanded their experiments for C<sub>2</sub>H<sub>6</sub>-C<sub>3</sub>H<sub>8</sub>, CH<sub>4</sub>-C<sub>2</sub>H<sub>6</sub>-C<sub>3</sub>H<sub>8</sub> and CH<sub>4</sub>-C<sub>2</sub>H<sub>6</sub>-  
 508 C<sub>3</sub>H<sub>8</sub>-iC<sub>4</sub>H<sub>10</sub> mixed hydrates. Based on the Raman spectra and confirmation of X-ray diffraction,  
 509 they reported that for C<sub>2</sub>H<sub>6</sub>-C<sub>3</sub>H<sub>8</sub> mixed hydrates, only structure II existed when the vapor  
 510 composition of ethane ranged from 28 to 73% mole fraction. They also stated that both molecules  
 511 occupied the 5<sup>12</sup>6<sup>4</sup> cages (sII large cages). Moreover, they concluded that the preferential  
 512 occupancy of 5<sup>12</sup>6<sup>4</sup> cages is C<sub>3</sub>H<sub>8</sub>>C<sub>2</sub>H<sub>6</sub>>CH<sub>4</sub>. For CH<sub>4</sub>-C<sub>2</sub>H<sub>6</sub>-C<sub>3</sub>H<sub>8</sub> hydrates, the initial methane  
 513 composition in gas phase was between 90 and 98% mole fraction. Their work showed that, at

514 final state, the composition of methane in gas phase increased, whereas the ethane and propane  
515 composition decreased. In hydrate phase, propane enriched more than other guest molecules.  
516 Furthermore, if the cage occupancy of ethane and propane was less than 33%, the methane  
517 molecules can occupy some  $5^{12}6^4$  cages. For the quaternary hydrate mixture, they reported the  
518 existence of structure II. In addition, all the molecules except methane, occupied the  $5^{12}6^4$  cages  
519 and the ratio is  $C_2H_6-C_3H_8-iC_4H_{10} = 2:3:5$ . They concluded that at a desired temperature, the  
520 larger molecules with lower dissociation pressure, enriched more in hydrate phase [77].

521 Schicks et al. [78] studied the phase behavior of methane-propane and methane-ethane-propane  
522 hydrates in a temperature range between 260 and 290 K and a pressure range from 1 to 6MPa.  
523 They investigated the phase transition, hydrate structure and composition by Raman spectroscopy  
524 and x-ray diffraction. They observed two different types of crystals after hydrate formation; light  
525 and dark. They reported the presence of occluded gas in the structure of light hydrate crystals.  
526 However, there was no evidence of the occluded gas in the dark crystals which was supposed to  
527 be structure II. Their approach demonstrated that there was a transformation process near the  
528 decomposition line. During the transformation, the crystal formation and decomposition was  
529 quick. They suggested that this is due to the occluded of free gas or water. Below this, they  
530 observed both structure I and II [78].

#### 531 **4.5.2. Issues of hydrate composition calculation from cage occupancy**

532 Although there are a lot of studies on the pure hydrate formers or kinetic investigation of mixed  
533 hydrates by microscopic measurements tools [79–86], there is still little research based on these  
534 tools to measure mixed hydrates composition at equilibrium. Furthermore, even in these pertinent  
535 studies, they sometimes did not mention clearly their experimental data on hydrate composition  
536 (reporting experimental results only on figures, for instance). Therefore, it was impossible to  
537 compare their experimental results with the thermodynamic model. In some studies, researchers  
538 measured the relative ratios of cage occupancy for mixtures based on Raman spectroscopy. Then,  
539 based on the statistical thermodynamics, they calculated absolute cage occupancy. Hydrate  
540 composition could be calculated based on the absolute cage occupancy [74]. Since this  
541 information was retrieved from statistical thermodynamics, they are of less interest for this  
542 review.

### 543 **5. Conclusion**

544 While equilibrium conditions of clathrate hydrates, such as temperature, pressure and gas phase  
545 composition have been widely studied, the hydrate composition is usually ignored due to the  
546 experimental difficulties, like the non-homogenous hydrate phase, water and free gas occlusion,  
547 etc. [12]. However, vital data for hydrate composition can be compiled from literature. This  
548 information provides comprehensive, representative, and additional knowledge about hydrate  
549 composition according to the different equilibrium conditions. Hence, this was the motivation to  
550 assemble the relevant research on the hydrate composition by different experimental procedures

551 and compare these methods via simulation based on the van der Waals and Platteeuw approach  
552 and Kihara potential for hydrate equilibrium pressure and composition.

553 Hydrate composition of binary mixtures of carbon dioxide, methane and nitrogen were usually  
554 studied since the idea of methane exploration from the hydrate resources by carbon dioxide  
555 isolation and gas separation was presented. Experimental data indicated that hydrate composition  
556 strongly depends on guest composition in gas phase. A small change in gas composition could  
557 lead to a substantial change in hydrate composition. Furthermore, the composition of heavier  
558 hydrocarbons (propane and butane) in the hydrate phase was significantly higher than in the gas  
559 phase.

560 Our simulations showed that generally, the thermodynamic model predicted adequately the  
561 hydrate equilibrium composition. In fact, the thermodynamic model had the best accordance with  
562 the experimental data obtained by the microscopic tools like Raman spectroscopy. This suggests  
563 that using these direct measurement techniques might help researchers to get closer to reality.  
564 Nevertheless, the existence of structural transition led to a significant deviation. Failure to predict  
565 structure change could be one of the main challenges for applying effectively the thermodynamic  
566 models.

567 Furthermore, at pressures higher than 7 MPa or when CO<sub>2</sub> was the minor component in hydrate  
568 phase, the deviation of the thermodynamic model from the experimental data was considerable.

569 Unfortunately, there were some cases which the agreement between the results of thermodynamic  
570 model and experimental data were not satisfactory. This might be explained by kinetic effects  
571 during the crystallization as well as the experimental methodology which could have a significant  
572 influence on the experiment. Furthermore, Bouillot and Herri reported that a small change of  
573 Kihara parameters had a considerable effect on the hydrate pressure and composition calculations  
574 [58]. Hence, it is essential to extend the experimental database in order to well optimize the  
575 Kihara parameters. Interestingly, there is still a lack of data concerning storage capacity of  
576 hydrates. This information could be used to re-design and develop chemical processes which the  
577 volume of gas stored in hydrate phase has been taken into account. Finally, consistent, reliable  
578 and extensive experimental data is still needed to examine the ability of thermodynamic modeling  
579 to predict hydrate composition as well as its developments.

## 580 **Acknowledgements**

581 The authors would like to thank Professor Christopher Yukna for his help in proofreading and his  
582 suggestions. Saheb Maghsoodloo Babakhani and Son Ho-Van are grateful to Ecole des Mines de  
583 Saint-Etienne for providing them Ph.D. scholarships.

## 584 **References**

- 585 [1] W.K. Burton, N. Cabrera, F.C. Frank, The Growth of Crystals and the Equilibrium Structure  
586 of their Surfaces, *Philos. Trans. R. Soc. Math. Phys. Eng. Sci.* 243 (1951) 299–358.  
587 doi:10.1098/rsta.1951.0006.
- 588 [2] P.B. Dharmawardhana, W.R. Parrish, E.D. Sloan, Experimental Thermodynamic Parameters  
589 for the Prediction of Natural Gas Hydrate Dissociation Conditions, *Ind. Eng. Chem.*  
590 *Fundam.* 19 (1980) 410–414. doi:10.1021/i160076a015.
- 591 [3] P. Englezos, N. Kalogerakis, P.D. Dholabhai, P.R. Bishnoi, Kinetics of formation of  
592 methane and ethane gas hydrates, *Chem. Eng. Sci.* 42 (1987) 2647–2658. doi:10.1016/0009-  
593 2509(87)87015-X.
- 594 [4] J.-M. Herri, F. Gruy, J.-S. Pic, M. Cournil, B. Cingotti, A. Siquin, Interest of in situ  
595 turbidimetry for the characterization of methane hydrate crystallization: application to the  
596 study of kinetic inhibitors, *Chem. Eng. Sci.* 54 (1999a) 1849–1858.
- 597 [5] A.K.M. Jamaluddin, N. Kalogerakis, P.R. Bishnoi, Hydrate plugging problems in undersea  
598 natural gas pipelines under shutdown conditions, *J. Pet. Sci. Eng.* 5 (1991) 323–335.  
599 doi:10.1016/0920-4105(91)90051-N.
- 600 [6] T. Maekawa, Phase equilibria for hydrate formation from binary mixtures of ethane,  
601 propane and noble gases, *Fluid Phase Equilibria.* 243 (2006) 115–120.  
602 doi:10.1016/j.fluid.2006.02.015.
- 603 [7] H.-J. Ng, D.B. Robinson, A Method for Predicting the Equilibrium Gas Phase Water  
604 Content in Gas-Hydrate Equilibrium, *Ind. Eng. Chem. Fundam.* 19 (1980) 33–36.  
605 doi:10.1021/i160073a006.
- 606 [8] J. Nixdorf, L.R. Oellrich, Experimental determination of hydrate equilibrium conditions for  
607 pure gases, binary and ternary mixtures and natural gases, *Fluid Phase Equilibria.* 139  
608 (1997) 325–333. doi:10.1016/S0378-3812(97)00141-6.
- 609 [9] T. Collett, J.-J. Bahk, R. Baker, R. Boswell, D. Divins, M. Frye, D. Goldberg, J. Husebø, C.  
610 Koh, M. Malone, M. Morell, G. Myers, C. Shipp, M. Torres, Methane Hydrates in Nature—  
611 Current Knowledge and Challenges, *J. Chem. Eng. Data.* 60 (2015) 319–329.  
612 doi:10.1021/je500604h.
- 613 [10] A. Demirbas, Methane hydrates as potential energy resource: Part 2 – Methane production  
614 processes from gas hydrates, *Energy Convers. Manag.* 51 (2010) 1562–1571.  
615 doi:10.1016/j.enconman.2010.02.014.
- 616 [11] Y.F. Makogon, Natural gas hydrates – A promising source of energy, *J. Nat. Gas Sci. Eng.* 2  
617 (2010) 49–59. doi:10.1016/j.jngse.2009.12.004.
- 618 [12] E.D. Sloan, C.A. Koh, *Clathrate Hydrates of Natural Gases*, 3rd ed., CRC Press, 2007.
- 619 [13] N.H. Duc, F. Chauvy, J.-M. Herri, CO<sub>2</sub> capture by hydrate crystallization – A potential  
620 solution for gas emission of steelmaking industry, *Energy Convers. Manag.* 48 (2007)  
621 1313–1322. doi:10.1016/j.enconman.2006.09.024.
- 622 [14] J.-M. Herri, A. Bouchemoua, M. Kwaterski, A. Fezoua, Y. Ouabbas, A. Cameirao, Gas  
623 hydrate equilibria for CO<sub>2</sub>–N<sub>2</sub> and CO<sub>2</sub>–CH<sub>4</sub> gas mixtures—Experimental studies and  
624 thermodynamic modelling, *Fluid Phase Equilibria.* 301 (2011) 171–190.  
625 doi:10.1016/j.fluid.2010.09.041.
- 626 [15] R. Kumar, H. Wu, P. Englezos, Incipient hydrate phase equilibrium for gas mixtures  
627 containing hydrogen, carbon dioxide and propane, *Fluid Phase Equilibria.* 244 (2006) 167–  
628 171. doi:10.1016/j.fluid.2006.04.008.
- 629 [16] P. Linga, R. Kumar, P. Englezos, The clathrate hydrate process for post and pre-combustion  
630 capture of carbon dioxide, *J. Hazard. Mater.* 149 (2007) 625–629.  
631 doi:10.1016/j.jhazmat.2007.06.086.

- 632 [17] J. Park, Y.-T. Seo, J. Lee, H. Lee, Spectroscopic analysis of carbon dioxide and nitrogen  
633 mixed gas hydrates in silica gel for CO<sub>2</sub> separation, *Catal. Today*. 115 (2006) 279–282.  
634 doi:10.1016/j.cattod.2006.02.059.
- 635 [18] C.-Y. Sun, G.-J. Chen, L.-W. Zhang, Hydrate phase equilibrium and structure for (methane  
636 + ethane + tetrahydrofuran + water) system, *J. Chem. Thermodyn.* 42 (2010) 1173–1179.  
637 doi:10.1016/j.jct.2010.04.021.
- 638 [19] Q. Sun, X. Guo, A. Liu, B. Liu, Y. Huo, G. Chen, Experimental Study on the Separation of  
639 CH<sub>4</sub> and N<sub>2</sub> via Hydrate Formation in TBAB Solution, *Ind. Eng. Chem. Res.* 50 (2011)  
640 2284–2288. doi:10.1021/ie101726f.
- 641 [20] H. Tajima, A. Yamasaki, F. Kiyono, Energy consumption estimation for greenhouse gas  
642 separation processes by clathrate hydrate formation, *Energy*. 29 (2004) 1713–1729.  
643 doi:10.1016/j.energy.2004.03.003.
- 644 [21] V.M. Vorotyntsev, V.M. Malyshev, P.G. Taraburov, G.M. Mochalov, Separation of Gas  
645 Mixtures by Continuous Gas Hydrate Crystallization, *Theor. Found. Chem. Eng.* 35 (2001)  
646 513–515. doi:10.1023/A:1012390423740.
- 647 [22] S.-P. Kang, J. Lee, Y. Seo, Pre-combustion capture of CO<sub>2</sub> by gas hydrate formation in  
648 silica gel pore structure, *Chem. Eng. J.* 218 (2013) 126–132. doi:10.1016/j.cej.2012.11.131.
- 649 [23] Q.-L. Ma, G.-J. Chen, C.-Y. Sun, Vapor–liquid–liquid–hydrate phase equilibrium  
650 calculation for multicomponent systems containing hydrogen, *Fluid Phase Equilibria*. 338  
651 (2013) 87–94. doi:10.1016/j.fluid.2012.11.002.
- 652 [24] S. Said, V. Govindaraj, J.-M. Herri, Y. Ouabbas, M. Khodja, M. Belloum, J.S. Sangwai, R.  
653 Nagarajan, A study on the influence of nanofluids on gas hydrate formation kinetics and  
654 their potential: Application to the CO<sub>2</sub> capture process, *J. Nat. Gas Sci. Eng.* 32 (2016) 95–  
655 108. doi:10.1016/j.jngse.2016.04.003.
- 656 [25] M. Yang, W. Jing, J. Zhao, Z. Ling, Y. Song, Promotion of hydrate-based CO<sub>2</sub> capture from  
657 flue gas by additive mixtures (THF (tetrahydrofuran) + TBAB (tetra-n-butyl ammonium  
658 bromide)), *Energy*. 106 (2016) 546–553. doi:10.1016/j.energy.2016.03.092.
- 659 [26] M. Yang, Y. Song, L. Jiang, Y. Zhao, X. Ruan, Y. Zhang, S. Wang, Hydrate-based  
660 technology for CO<sub>2</sub> capture from fossil fuel power plants, *Appl. Energy*. 116 (2014) 26–40.  
661 doi:10.1016/j.apenergy.2013.11.031.
- 662 [27] T. Yu, T. Sato, T. Nakashima, M. Inui, H. Oyama, An integrated model for CO<sub>2</sub> hydrate  
663 formation in sand sediments for sub-seabed CO<sub>2</sub> storage, *Int. J. Greenh. Gas Control*. 52  
664 (2016) 250–269. doi:10.1016/j.ijggc.2016.07.009.
- 665 [28] J. Zheng, P. Zhang, P. Linga, Semiclathrate hydrate process for pre-combustion capture of  
666 CO<sub>2</sub> at near ambient temperatures, *Appl. Energy*. 194 (2017) 267–278.  
667 doi:10.1016/j.apenergy.2016.10.118.
- 668 [29] J. Zheng, Y.K. Lee, P. Babu, P. Zhang, P. Linga, Impact of fixed bed reactor orientation,  
669 liquid saturation, bed volume and temperature on the clathrate hydrate process for pre-  
670 combustion carbon capture, *J. Nat. Gas Sci. Eng.* 35, Part B (2016) 1499–1510.  
671 doi:10.1016/j.jngse.2016.03.100.
- 672 [30] D.-L. Zhong, J.-L. Wang, Y.-Y. Lu, Z. Li, J. Yan, Precombustion CO<sub>2</sub> capture using a  
673 hybrid process of adsorption and gas hydrate formation, *Energy*. 102 (2016) 621–629.  
674 doi:10.1016/j.energy.2016.02.135.
- 675 [31] P. Babu, R. Kumar, P. Linga, Unusual behavior of propane as a co-guest during hydrate  
676 formation in silica sand: Potential application to seawater desalination and carbon dioxide  
677 capture, *Chem. Eng. Sci.* 117 (2014) 342–351. doi:10.1016/j.ces.2014.06.044.

- 678 [32] H. Fakharian, H. Ganji, A. Naderifar, Desalination of high salinity produced water using  
679 natural gas hydrate, *J. Taiwan Inst. Chem. Eng.* 72 (2017) 157–162.  
680 doi:10.1016/j.jtice.2017.01.025.
- 681 [33] S. Han, Y.-W. Rhee, S.-P. Kang, Investigation of salt removal using cyclopentane hydrate  
682 formation and washing treatment for seawater desalination, *Desalination*. 404 (2017) 132–  
683 137. doi:10.1016/j.desal.2016.11.016.
- 684 [34] K.C. Kang, P. Linga, K. Park, S.-J. Choi, J.D. Lee, Seawater desalination by gas hydrate  
685 process and removal characteristics of dissolved ions ( $\text{Na}^+$ ,  $\text{K}^+$ ,  $\text{Mg}^{2+}$ ,  $\text{Ca}^{2+}$ ,  $\text{B}_3^+$ ,  $\text{Cl}^-$ ,  
686  $\text{SO}_4^{2-}$ ), *Desalination*. 353 (2014) 84–90. doi:10.1016/j.desal.2014.09.007.
- 687 [35] Y.-N. Lv, S.-S. Wang, C.-Y. Sun, J. Gong, G.-J. Chen, Desalination by forming hydrate  
688 from brine in cyclopentane dispersion system, *Desalination*. 413 (2017) 217–222.  
689 doi:10.1016/j.desal.2017.03.025.
- 690 [36] M. Yang, J. Zheng, W. Liu, Y. Liu, Y. Song, Effects of  $\text{C}_3\text{H}_8$  on hydrate formation and  
691 dissociation for integrated  $\text{CO}_2$  capture and desalination technology, *Energy*. 93, Part 2  
692 (2015) 1971–1979. doi:10.1016/j.energy.2015.10.076.
- 693 [37] J. Zheng, M. Yang, Y. Liu, D. Wang, Y. Song, Effects of cyclopentane on  $\text{CO}_2$  hydrate  
694 formation and dissociation as a co-guest molecule for desalination, *J. Chem. Thermodyn.*  
695 104 (2017) 9–15. doi:10.1016/j.jct.2016.09.006.
- 696 [38] S. Ho-Van, B. Bouillot, J. Douzet, S.M. Babakhani, J.M. Herri, Experimental measurement  
697 and thermodynamic modeling of cyclopentane hydrates with  $\text{NaCl}$ ,  $\text{KCl}$ ,  $\text{CaCl}_2$ , or  $\text{NaCl}$ -  
698  $\text{KCl}$  present, *AIChE J.* In press (2018). doi:10.1002/aic.16067.
- 699 [39] A. Erfani, E. Fallah-Jokandan, F. Varaminian, Effects of non-ionic surfactants on formation  
700 kinetics of structure H hydrate regarding transportation and storage of natural gas, *J. Nat.*  
701 *Gas Sci. Eng.* 37 (2017) 397–408. doi:10.1016/j.jngse.2016.11.058.
- 702 [40] J. Javanmardi, K. Nasrifar, S.H. Najibi, M. Moshfeghian, Economic evaluation of natural  
703 gas hydrate as an alternative for natural gas transportation, *Appl. Therm. Eng.* 25 (2005)  
704 1708–1723. doi:10.1016/j.applthermaleng.2004.10.009.
- 705 [41] J. Lim, E. Kim, Y. Seo, Dual inhibition effects of diamines on the formation of methane gas  
706 hydrate and their significance for natural gas production and transportation, *Energy*  
707 *Convers. Manag.* 124 (2016) 578–586. doi:10.1016/j.enconman.2016.07.054.
- 708 [42] S. Maghsoodloo Babakhani, A. Alamdari, Effect of maize starch on methane hydrate  
709 formation/dissociation rates and stability, *J. Nat. Gas Sci. Eng.* 26 (2015) 1–5.  
710 doi:10.1016/j.jngse.2015.05.026.
- 711 [43] H. Mimachi, S. Takeya, A. Yoneyama, K. Hyodo, T. Takeda, Y. Gotoh, T. Murayama,  
712 Natural gas storage and transportation within gas hydrate of smaller particle: Size  
713 dependence of self-preservation phenomenon of natural gas hydrate, *Chem. Eng. Sci.* 118  
714 (2014) 208–213. doi:10.1016/j.ces.2014.07.050.
- 715 [44] Z. Taheri, M.R. Shabani, K. Nazari, A. Mehdizaheh, Natural gas transportation and storage  
716 by hydrate technology: Iran case study, *J. Nat. Gas Sci. Eng.* 21 (2014) 846–849.  
717 doi:10.1016/j.jngse.2014.09.026.
- 718 [45] I. Chatti, A. Delahaye, L. Fournaison, J.-P. Petitet, Benefits and drawbacks of clathrate  
719 hydrates: a review of their areas of interest, *Energy Convers. Manag.* 46 (2005) 1333–1343.  
720 doi:10.1016/j.enconman.2004.06.032.
- 721 [46] J.-M. Herri, M. Cournil, E. Chassefiere, Thermodynamic modelling of clathrate hydrates in  
722 the atmosphere of Mars, HAL. (2011). <https://hal.archives-ouvertes.fr/hal-00617450>.
- 723 [47] J.-M. Herri, E. Chassefière, Carbon dioxide, argon, nitrogen and methane clathrate hydrates:  
724 Thermodynamic modelling, investigation of their stability in Martian atmospheric

725 conditions and variability of methane trapping, *Planet. Space Sci.* 73 (2012) 376–386.  
726 doi:10.1016/j.pss.2012.07.028.

727 [48] S.L. Miller, W.D. Smythe, Carbon dioxide clathrate in the martian ice cap, *Science*. 170  
728 (1970) 531–533. doi:10.1126/science.170.3957.531.

729 [49] M.N. Khan, P. Warriar, C.J. Peters, C.A. Koh, Review of vapor-liquid equilibria of gas  
730 hydrate formers and phase equilibria of hydrates, *J. Nat. Gas Sci. Eng.* 35, Part B (2016)  
731 1388–1404. doi:10.1016/j.jngse.2016.06.043.

732 [50] A.Y. Manakov, A.D. Duchkov, Laboratory modeling of hydrate formation in rock  
733 specimens (a review), *Russ. Geol. Geophys.* 58 (2017) 240–252.  
734 doi:10.1016/j.rgg.2016.01.023.

735 [51] S. Shahnazar, N. Hasan, Gas hydrate formation condition: Review on experimental and  
736 modeling approaches, *Fluid Phase Equilibria*. 379 (2014) 72–85.  
737 doi:10.1016/j.fluid.2014.07.012.

738 [52] Y. Song, L. Yang, J. Zhao, W. Liu, M. Yang, Y. Li, Y. Liu, Q. Li, The status of natural gas  
739 hydrate research in China: A review, *Renew. Sustain. Energy Rev.* 31 (2014) 778–791.  
740 doi:10.1016/j.rser.2013.12.025.

741 [53] Q. Sun, Y.T. Kang, Review on CO<sub>2</sub> hydrate formation/dissociation and its cold energy  
742 application, *Renew. Sustain. Energy Rev.* 62 (2016) 478–494.  
743 doi:10.1016/j.rser.2016.04.062.

744 [54] Z. Yin, Z.R. Chong, H.K. Tan, P. Linga, Review of gas hydrate dissociation kinetic models  
745 for energy recovery, *J. Nat. Gas Sci. Eng.* 35, Part B (2016) 1362–1387.  
746 doi:10.1016/j.jngse.2016.04.050.

747 [55] J.H. van der Waals, J.C. Platteeuw, Clathrate Solutions, in: I. Prigogine (Ed.), *Adv. Chem.*  
748 *Phys.*, John Wiley & Sons, Inc., Hoboken, NJ, USA, 1959: pp. 1–57.  
749 <http://doi.wiley.com/10.1002/9780470143483.ch1> (accessed December 22, 2015).

750 [56] Y.P. Handa, J.S. Tse, Thermodynamic properties of empty lattices of structure I and  
751 structure II clathrate hydrates, *J. Phys. Chem.* 90 (1986) 5917–5921.  
752 doi:10.1021/j100280a092.

753 [57] D. Le Quang, D. Le Quang, B. Bouillot, J.-M. Herri, P. Glenat, P. Duchet-Suchaux,  
754 Experimental procedure and results to measure the composition of gas hydrate, during  
755 crystallization and at equilibrium, from N<sub>2</sub>–CO<sub>2</sub>–CH<sub>4</sub>–C<sub>2</sub>H<sub>6</sub>–C<sub>3</sub>H<sub>8</sub>–C<sub>4</sub>H<sub>10</sub> gas mixtures,  
756 *Fluid Phase Equilibria*. (2015). doi:10.1016/j.fluid.2015.10.022.

757 [58] B. Bouillot, J.-M. Herri, Framework for clathrate hydrate flash calculations and implications  
758 on the crystal structure and final equilibrium of mixed hydrates, *Fluid Phase Equilibria*.  
759 (2015). doi:10.1016/j.fluid.2015.10.023.

760 [59] V. McKoy, O. Sinanoğlu, Theory of Dissociation Pressures of Some Gas Hydrates, *J.*  
761 *Chem. Phys.* 38 (1963) 2946. doi:10.1063/1.1733625.

762 [60] J.E.D. Sloan, *Clathrate Hydrates of Natural Gases*, Second Edition, Revised and Expanded,  
763 CRC Press, 1998.

764 [61] S. Maghsoodloo Babakhani, B. Bouillot, J. Douzet, S. Ho-Van, J.M. Herri, A new approach  
765 of studying mixed gas hydrates involving propane at non-equilibrium conditions and final  
766 state: An experimental study and modeling, *Chem. Eng. Sci.* (2018).  
767 doi:10.1016/j.ces.2018.01.017.

768 [62] J. Jhaveri, D.B. Robinson, Hydrates in the methane-nitrogen system, *Can. J. Chem. Eng.* 43  
769 (1965) 75–78. doi:10.1002/cjce.5450430207.

- 770 [63] T. Kawasaki, K. Kikuchi, D. Terasaki, T. Okui, K. Myata, H. Hirayama, M. Ihara,  
771 Composition of Guests in Hydrates from Gas Mixture, in: Yokohama, Japan, 2002: pp. 424–  
772 427.
- 773 [64] S.-P. Kang, H. Lee, C.-S. Lee, W.-M. Sung, Hydrate phase equilibria of the guest mixtures  
774 containing CO<sub>2</sub>, N<sub>2</sub> and tetrahydrofuran, *Fluid Phase Equilibria*. 185 (2001) 101–109.  
775 doi:10.1016/S0378-3812(01)00460-5.
- 776 [65] K. Ohgaki, K. Takano, H. Sangawa, T. Matsubara, S. Nakano, Methane exploitation by  
777 carbon dioxide from gas hydrates. Phase equilibria for CO<sub>2</sub>-CH<sub>4</sub> mixed hydrate system., *J.*  
778 *Chem. Eng. Jpn.* 29 (1996) 478–483. doi:10.1252/jcej.29.478.
- 779 [66] S. Angus, J.B. Armstrong, K.M. de Reuck, R.D. McCarthy, R.T. Jacobsen, W. Wagner,  
780 International thermodynamic tables of the fluid state. Methane 5 5, 1978.
- 781 [67] S. Angus, B. Armstrong, K.M. de Reuck, International thermodynamic tables of the fluid  
782 state: carbon dioxide, Pergamon Press, Oxford; New York, 1976.
- 783 [68] V. Belandria, A. Eslamimanesh, A.H. Mohammadi, P. Théveneau, H. Legendre, D. Richon,  
784 Compositional Analysis and Hydrate Dissociation Conditions Measurements for Carbon  
785 Dioxide + Methane + Water System, *Ind. Eng. Chem. Res.* 50 (2011) 5783–5794.  
786 doi:10.1021/ie101959t.
- 787 [69] V. Belandria, A. Eslamimanesh, A.H. Mohammadi, D. Richon, Gas Hydrate Formation in  
788 Carbon Dioxide + Nitrogen + Water System: Compositional Analysis of Equilibrium  
789 Phases, *Ind. Eng. Chem. Res.* 50 (2011) 4722–4730. doi:10.1021/ie101635k.
- 790 [70] Y.-T. Seo, S.-P. Kang, H. Lee, C.-S. Lee, W.-M. Sung, Hydrate phase equilibria for gas  
791 mixtures containing carbon dioxide: A proof-of-concept to carbon dioxide recovery from  
792 multicomponent gas stream, *Korean J. Chem. Eng.* 17 (2000) 659–667.
- 793 [71] H.-J. Ng, Hydrate Phase Composition for Multicomponent Gas Mixtures, *Ann. N. Y. Acad.*  
794 *Sci.* 912 (2000) 1034–1039. doi:10.1111/j.1749-6632.2000.tb06858.x.
- 795 [72] A.K. Sum, R.C. Burruss, E.D. Sloan, Measurement of Clathrate Hydrates via Raman  
796 Spectroscopy, *J. Phys. Chem. B.* 101 (1997) 7371–7377. doi:10.1021/jp970768e.
- 797 [73] S. Subramanian, A. Ballard, R. Kini, S. Dec, E. Sloan, Structural transitions in  
798 methane+ethane gas hydrates — Part I: upper transition point and applications, *Chem. Eng.*  
799 *Sci.* 55 (2000) 5763–5771. doi:10.1016/S0009-2509(00)00162-7.
- 800 [74] S. Subramanian, R.A. Kini, S.F. Dec, E.D. Sloan, Evidence of structure II hydrate formation  
801 from methane+ethane mixtures, *Chem. Eng. Sci.* 55 (2000) 1981–1999. doi:10.1016/S0009-  
802 2509(99)00389-9.
- 803 [75] Y.-T. Seo, H. Lee, Structure and Guest Distribution of the Mixed Carbon Dioxide and  
804 Nitrogen Hydrates As Revealed by X-ray Diffraction and <sup>13</sup>C NMR Spectroscopy, *J. Phys.*  
805 *Chem. B.* 108 (2004) 530–534. doi:10.1021/jp0351371.
- 806 [76] T. Uchida, S. Takeya, Y. Kamata, I.Y. Ikeda, J. Nagao, T. Ebinuma, H. Narita, O.  
807 Zatsepina, B.A. Buffett, Spectroscopic Observations and Thermodynamic Calculations on  
808 Clathrate Hydrates of Mixed Gas Containing Methane and Ethane: Determination of  
809 Structure, Composition and Cage Occupancy, *J. Phys. Chem. B.* 106 (2002) 12426–12431.  
810 doi:10.1021/jp025884i.
- 811 [77] T. Uchida, S. Takeya, Y. Kamata, R. Ohmura, H. Narita, Spectroscopic Measurements on  
812 Binary, Ternary, and Quaternary Mixed-Gas Molecules in Clathrate Structures, *Ind. Eng.*  
813 *Chem. Res.* 46 (2007) 5080–5087. doi:10.1021/ie070153w.
- 814 [78] J.M. Schicks, R. Naumann, J. Erzinger, K.C. Hester, C.A. Koh, E.D. Sloan, Phase  
815 Transitions in Mixed Gas Hydrates: Experimental Observations versus Calculated Data, *J.*  
816 *Phys. Chem. B.* 110 (2006) 11468–11474. doi:10.1021/jp0612580.

- 817 [79] D.W. Davidson, S.K. Garg, S.R. Gough, R.E. Hawkins, J.A. Ripmeester, Characterization  
818 of natural gas hydrates by nuclear magnetic resonance and dielectric relaxation, *Can. J.*  
819 *Chem.* 55 (1977) 3641–3650. doi:10.1139/v77-512.
- 820 [80] J.A. Ripmeester, C.I. Ratcliffe, The Diverse Nature of Dodecahedral Cages in Clathrate  
821 Hydrates As Revealed by <sup>129</sup>Xe and <sup>13</sup>C NMR Spectroscopy: CO<sub>2</sub> as a Small-Cage  
822 Guest, *Energy Fuels.* 12 (1998) 197–200. doi:10.1021/ef970171y.
- 823 [81] S. Nakano, M. Moritoki, K. Ohgaki, High-Pressure Phase Equilibrium and Raman  
824 Microprobe Spectroscopic Studies on the CO<sub>2</sub> Hydrate System, *J. Chem. Eng. Data.* 43  
825 (1998) 807–810. doi:10.1021/je9800555.
- 826 [82] I.L. Moudrakovski, G.E. McLaurin, C.I. Ratcliffe, J.A. Ripmeester, Methane and Carbon  
827 Dioxide Hydrate Formation in Water Droplets: Spatially Resolved Measurements from  
828 Magnetic Resonance Microimaging, *J. Phys. Chem. B.* 108 (2004) 17591–17595.  
829 doi:10.1021/jp0473220.
- 830 [83] S. Subramanian, E.D. Sloan, Microscopic Measurements and Modeling of Hydrate  
831 Formation Kinetics, *Ann. N. Y. Acad. Sci.* 912 (2006) 583–592. doi:10.1111/j.1749-  
832 6632.2000.tb06813.x.
- 833 [84] S. Gao, W.G. Chapman, W. House, NMR and Viscosity Investigation of Clathrate Hydrate  
834 Formation and Dissociation, *Ind. Eng. Chem. Res.* 44 (2005) 7373–7379.  
835 doi:10.1021/ie050464b.
- 836 [85] K.C. Hester, T.A. Strobel, E.D. Sloan, C.A. Koh, A. Huq, A.J. Schultz, Molecular  
837 Hydrogen Occupancy in Binary THF–H<sub>2</sub> Clathrate Hydrates by High Resolution Neutron  
838 Diffraction, *J. Phys. Chem. B.* 110 (2006) 14024–14027. doi:10.1021/jp063164w.
- 839 [86] R. Kumar, P. Englezos, I. Moudrakovski, J.A. Ripmeester, Structure and composition of  
840 CO<sub>2</sub>/H<sub>2</sub> and CO<sub>2</sub>/H<sub>2</sub>/C<sub>3</sub>H<sub>8</sub> hydrate in relation to simultaneous CO<sub>2</sub> capture and H<sub>2</sub>  
841 production, *AIChE J.* 55 (2009) 1584–1594. doi:10.1002/aic.11844.  
842